A Comprehensive Analysis of 5G Heterogeneous Cellular Systems operating over κ-μ Shadowed Fading Channels

Published in:

Document Version:
Publisher's PDF, also known as Version of record

Queen's University Belfast - Research Portal:
Link to publication record in Queen's University Belfast Research Portal

A Comprehensive Analysis of 5G Heterogeneous Cellular Systems operating over κ-μ Shadowed Fading Channels

Young Jin Chun, *Member, IEEE,* Simon L. Cotton, *Senior Member, IEEE,* Harpreet S. Dhillon, *Member, IEEE,* F. Javier Lopez-Martinez, *Member, IEEE,* Jose F. Paris, *Senior Member, IEEE,* Seong Ki Yoo, *Student Member, IEEE*

Abstract—Emerging cellular technologies such as those proposed for use in 5G communications will accommodate a wide range of usage scenarios with diverse link requirements. This will include the necessity to operate over a versatile set of wireless channels ranging from indoor to outdoor, from line-of-sight (LOS) to non-LOS, and from circularly symmetric scattering to environments which promote the clustering of scattered multipath waves. Unfortunately, many of the conventional fading models lack the flexibility to account for such disparate signal propagation mechanisms. To bridge the gap between theory and practical channels, we consider κ-μ shadowed fading, which contains as special cases the majority of the linear fading models proposed in the open literature. In particular, we propose an analytic framework to evaluate the average of an arbitrary function of the signal-to-noise-plus-interference ratio (SINR) over κ-μ shadowed fading channels by using a simplified orthogonal expression with tools from stochastic geometry. Using the proposed method, we evaluate the spectral efficiency, moments of the SINR, and outage probability of a K-tier HetNet with K classes of BSs, differing in terms of the transmit power, BS density, shadowing and fading. Building upon these results, we provide important new insights into the network performance of these emerging wireless applications while considering a diverse range of fading conditions and link qualities.

Index Terms—Stochastic geometry, Poisson point process, Composite fading, HetNets, κ-μ shadowed.

Y. J. Chun, S. L. Cotton and S. K. Yoo are with the Wireless Communications Laboratory, ECIT Institute, Queen's University Belfast, Belfast, BT3 9DT, U.K. (e-mail: y.chun@qub.ac.uk, simon.cotton@qub.ac.uk, syoo02@qub.ac.uk).

H. S. Dhillon is with Wireless@VT, Department of Electrical and Computer Engineering, Virginia Tech, Blacksburg, VA, 24060, USA (e-mail: hdhillon@vt.edu).

F. J. Lopez-Martinez and J. F. Paris are with Departmento de Ingenieria de Comunicaciones, Universidad de Malaga, 29071 Malaga, Spain. (e-mail: fjlopezm@ic.uma.es, paris@ic.uma.es).

Color versions of one or more of the figures in this paper are available online at http://ieeexplore.ieee.org.

Digital Object Identifier xx.xxxx/TWC.2017.xxxxxxx

I. INTRODUCTION

To meet the ever-increasing demand for data on the move, telecommunications industries, as well as global standardization entities, are actively driving the research and development of the fifth generation (5G) of wireless communications. It is forecast that this new networking paradigm will provide 1000 fold gains in capacity over the next decade and data rates exceeding 10 Gigabit/s while achieving latencies of less than 1 millisecond [1], [2]. To make this possible, 5G communications will utilize densely deployed small cells to achieve high spectral efficiency while harnessing all available spectrum resources, including opportunities offered by millimeter-wave frequencies. Key to the successful operation of 5G communications will be the unification of dissimilar networking technologies. This will create a diverse range of link requirements and the necessity for wireless devices to operate over a versatile set of channels ranging from indoor to outdoor, from line-of-sight (LOS) to non-LOS (NLOS), and from homogeneous diffuse scattering to those which promote the clustering of scattered multipath waves.

A range of tools developed within the framework of stochastic geometry have been used to capture the irregularity and heterogeneity of 5G wireless networks with considerable success. Specifically, stochastic geometry assumes that the locations of all wireless nodes are endowed with a spatial point process [3]. Such an approach captures the topological randomness in the network geometry, allows the use of well-established mathematical tools, offers high analytical flexibility and achieves an accurate performance evaluation [4]. A common assumption made within this scheme is that the nodes are distributed according to a Poisson point process (PPP). Using this supposition, the probability density function (PDF) of the aggregate interference and the outage probability were analyzed for cellular networks in [5], [6], which were then generalized to the case of heterogeneous cellular networks (HetNets) in [7]–[11][1].

Much of the existing published work on stochastic geometry has focused on the Rayleigh distribution as the de facto small-scale fading model, owing to its simplicity and tractability.

---

[1]The aforementioned results represent only a subset of the related studies in stochastic geometry. The interested reader is directed to the work presented in [12]–[14] and the references therein for a more detailed overview of stochastic geometry.

Several approaches have been proposed to derive the signal-to-noise-plus-interference ratio (SINR) distributions for general fading environments. For instance, in [15]–[19] the conversion method, which is based on displacement theorem, was used. This method treats the channel randomness as a perturbation in the location of the transmitter and transforms the original network with arbitrary fading into an equivalent network without fading. Although the conversion method can be applied to any fading distribution, it is more tractable for handling large-scale shadowing effects. Specifically, if one applies the conversion method to small-scale fading, the resulting equivalent model will have no fading, thereby the Laplace transform-based approach can not be utilized. An alternative approach to address general fading scenarios uses the series representation method [20], [21]. This approach expresses the interference functionals as an infinite series of higher order derivative terms given by the Laplace transform of the interference power. While the series representation method provides a tractable alternate for handling general fading, it often leads to situations where it is difficult to derive closed form expressions. Numerically evaluating a higher order derivative is also complex and prone to floating-point rounding errors [22].

Aside from the small-scale fading, random shadowing due to obstacles in the local environment or human body movements (in the case of user equipments) can impact link performance by causing fluctuations in the received signal. Shadowing affects the transmission performance, which will be especially pertinent in a dense network or millimeter-wave links. Hence, the combined effect of small-scale and shadowed fading needs to be properly addressed in 5G communications design. In this respect, composite channel models have been proposed in [23]–[27]. In [23], the shadowed Nakagami fading distribution was first proposed by combining Nakagami-m multipath fading and lognormal distributed shadowing. Later, [24] introduced the generalized-K model by approximating the shadowing model in [23] using the gamma distribution to improve analytical tractability. Traditional composite channel models (referred to as *multiplicative shadow fading models*) assume that the shadowing affects the dominant components and the scattered waves equally, whereas, in practice, the shadowing often only occurs on the dominant components, which gives rise to a different kind of composite model, often referred to as a *LOS shadow fading model*. To model shadowing in LOS channels, [25] proposed the Rician shadowed fading model by assuming a Rician distribution for the multipath fading and Nakagami-m distribution for the LOS shadowing. More recently, [26], [27] proposed κ-μ shadowed fading model by assuming κ-μ multipath fading with shadowing of the dominant component.

The κ-μ shadowed fading model is an attractive proposition, not just due to its excellent fit to the fading observed in a range of real-world applications (e.g. device-to-device [27], underwater acoustic [28], body-centric fading channels [29], etc.) but also its extreme versatility. More precisely, it is able to account for most of the popular fading distributions utilized in the literature. Motivated by the comprehensive nature of the κ-μ shadowed fading model, we use it along with a stochastic geometric framework to derive the downlink SINR distribution

of a typical user in a K-tier HetNet with K classes of BSs, differing in terms of the transmit power, BS density, shadowing and fading characteristics. We evaluate the average of an arbitrary function of the SINR, which can be easily applied to other network models. For instance, it may be utilized to evaluate any performance measure that can be represented as a function of SINR, *e.g.*, the spectral efficiency, outage probability, moments of the SINR, and error probability.

The main contributions of this paper may be summarized as follows.

1) The main difficulty with incorporating generalized fading models into stochastic geometry frameworks is the lack of tractability in expressing the PDF of the interference. In general, it is more convenient to express the metrics of interest in terms of the Laplace transform of the interference. Nonetheless, this presents significant challenges when extending the analyses from Rayleigh fading to the more general fading models. We overcome this problem by analyzing the Laplace transform of the interference over κ-μ shadowed channels to characterize the distribution of the interference from cellular user equipment (UE). It is worth highlighting that this model encompasses as special cases, the majority of the fading models proposed in the literature, including Rayleigh, Rician, Nakagami-m, Nakagami-q, One-sided Gaussian, κ-μ, η-μ, and Rician shadowed distribution to name but a few.

2) We use tools from stochastic geometry to evaluate the distribution of the SINR, coverage probability and average rate for κ-μ shadowed fading. We also propose a numerically efficient method to calculate the average of an arbitrary function of the SINR.

3) We present numerical simulation results which provide useful insights into the performance of cellular networks for different fading conditions. In particular, we observe the trade-off relation between the rate and average SINR based on the channel parameters, such as the intensity of dominant signal components, the number of scattering clusters, and shadowing effect. This information will be of paramount importance to those responsible for designing future 5G network infrastructure to ensure that adequate service can be provided.

This paper is organized as follows. In Section II, the system model and assumptions are introduced. We then apply an orthogonal expansion to κ-μ shadowed PDF in Section III, characterize the interference distribution in Section IV, and introduce a novel analytical framework in Section V. Following this, in Section VI, we present both numerical and simulated results to validate the analysis. Finally, Section VII concludes this paper.

II. SYSTEM MODEL

A. Network Model

We consider the downlink of a K-tier HetNet where randomly distributed small-cell BSs, such as pico or femtocell BSs, are overlaid on a network of macrocell BSs. The BSs of each tier may differ in terms of transmit power, spatial

density and cell-selection bias. The locations of the k-th tier BSs are modeled by an independent, homogeneous PPP Φ_k with density λ_k and the union of K point processes constitutes the K-tier HetNet $\Phi = \underset{k \in \mathcal{K}}{\cup} \Phi_k$ where $\mathcal{K} = \{1, 2, \ldots, K\}$. The locations of the UEs are modeled by a homogeneous PPP $\Phi^{(u)}$ with density $\lambda^{(u)}$ that is independent of Φ. Orthogonal multiple access is employed at each cell by allocating mutually orthogonal resource blocks to each UE, implying no intra-cell interference within a cell. Without loss of generality, we assume that a typical UE is located at the origin and each BS has an infinitely backlogged queue. The received power at a typical UE from a k-th tier BS $x_k \in \Phi_k$[2] is given by

$$P_{x_k} = P_k H_{x_k} \left(\tau \|x_k\|^{-\alpha} \right) = P_k h_{x_k} \chi_{x_k} \left(\tau \|x_k\|^{-\alpha} \right), \quad (1)$$

where a multiplicative channel model $H_{x_k} = h_{x_k} \chi_{x_k}$ with large-scale shadowing χ and small-scale fading h is utilized in the second equality, P_k is the transmit power of the k-th tier BS, α is the path-loss exponent ($\alpha > 2$) and τ is the path-loss intercept at a link-length $\|x\| = 1$.

B. Cell Association Policy

We assume a general cell association model where all BSs allow open access and each UE connects to the BS that provides the highest *long-term biased received power* (LRP)[3] without small-scale fading as written below

Typical UE associates to a k-th tier BS $x_k^* \in \Phi_k$

$$\begin{aligned} \leftrightarrow x_k^* &= \arg \max_{j \in \mathcal{K}, \, x \in \Phi_j} B_j P_j \chi_j \|x\|^{-\alpha} \\ &= \arg \max_{j \in \mathcal{K}, \, y \in \Phi_j^{(e)}} B_j P_j \|y\|^{-\alpha}, \end{aligned} \quad (2)$$

where B_j is the bias connecting to the j-th tier BS ($B_j > 0$) and a change of variable, *i.e.*, $y = \chi_j^{-\frac{1}{\alpha}} x$, is applied in the last equality. For a single tier network, (2) is equivalent to connecting with the closest BS.

Due to the displacement theorem [18, Lemma 1], the mapping between x and y converts a PPP $\Phi_j = \{x\}$ with density λ_j into a new homogeneous PPP $\Phi_j^{(e)} = \{y\}$ with density $\lambda_j^{(e)} = \lambda_j \mathbb{E}[\chi_j^\delta]$ where $\delta = \frac{2}{\alpha}$. Thereby, the original network model Φ with large-scale shadowing χ can be equivalently expressed as the network $\Phi^{(e)} = \underset{j \in \mathcal{K}}{\cup} \Phi_j^{(e)}$ without large-scale shadowing where the effect of large-scale shadowing is now incorporated through an appropriate scaling in the density $\lambda_j \to \lambda_j^{(e)}$. Given that the serving BS belongs to the k-th tier, the SINR at a typical UE can be formulated as follows

$$\begin{aligned} \mathrm{SINR}_k &= \frac{P_k \chi_{x_k^*} h_{x_k^*} \|x_k^*\|^{-\alpha}}{N + \sum_{j \in \mathcal{K}} \sum_{x \in \Phi_j \backslash \{x_k^*\}} P_j \chi_x h_x \|x\|^{-\alpha}} \\ &\overset{d}{=} \frac{h_{y_k^*} \|y_k^*\|^{-\alpha}}{\hat{N} + \sum_{j \in \mathcal{K}} \sum_{y \in \Phi_j^{(e)} \backslash \{y_k^*\}} \hat{P}_j h_y \|y\|^{-\alpha}}, \end{aligned} \quad (3)$$

---

[2] x_k denotes both the node and the coordinates of the BS.
[3] The interested reader is referred to [7], [18], [19] for a detailed description of the long-term association scheme.

where $\overset{d}{=}$ denotes equivalence in distribution, which follows from [18, Lemma 1], x_k^* represents the location of the associated k-tier BS, $\Phi \backslash \{x_k^*\}$ denote the set of interfering BSs, $\hat{P}_j = \frac{P_j}{P_k}$ represents the ratio between the transmit power of the interfering and serving BS and $\hat{N} = \frac{N}{P_k} = \frac{N_0 W}{\tau P_k}$ is determined by the noise power spectral density N_0, bandwidth W, transmit power of the associated BS P_k, and the reference path-loss τ at a unit distance. Similarly, we denote $\hat{B}_j = \frac{B_j}{B_k}$ as the ratio between the bias factor of the interfering and serving BS and $I \triangleq \sum_{j \in \mathcal{K}} \sum_{y \in \Phi_j^{(e)} \backslash \{y_k^*\}} \hat{P}_j h_y \|y\|^{-\alpha}$ as the aggregate interference normalized by the transmit power of the serving BS. Since the cell association policy in (2) is independent of the small-scale fading distribution h, the probability that a typical UE connects to the k-th tier BS, denoted as $\mathcal{P}_k$, and the PDF of the link length $\|y_k^*\|$ can be evaluated as below

$$\mathcal{P}_k = \frac{\lambda_k \mathbb{E}\left[\chi_k^\delta\right]}{\sum_{j \in \mathcal{K}} \lambda_j \mathbb{E}\left[\chi_j^\delta\right] \hat{P}_j^\delta \hat{B}_j^\delta},$$

$$f_{\|y_k^*\|}(r) = \frac{2\pi \lambda_k \mathbb{E}\left[\chi_k^\delta\right]}{\mathcal{P}_k} r \exp\left(-\sum_{j \in \mathcal{K}} \pi r^2 \lambda_j \mathbb{E}\left[\chi_j^\delta\right] \hat{P}_j^\delta \hat{B}_j^\delta\right),$$

$$(4)$$

where $\delta = \frac{2}{\alpha}$ and (4) follows directly from [7, Lemma 1] and [18, Lemma 2].

C. Channel Model

Due to the wide range of use cases provisioned for 5G communications, conventional cellular channel models which typically only consider a single source of shadowing (e.g. large-scale shadowing) are unlikely to be general enough. In reality, it is probable that cellular applications will encounter multiple independent types of shadowing which may or may not occur concurrently. For example in the downlink scenario, the signal transmitted from the BS to the UE will undergo two key types of shadowing, the first of which is large-scale shadowing, denoted here by χ, which is induced due to large terrestrial objects *e.g.* buildings or hills, which can cause a random fluctuation in the total signal power. In cellular networks, the BSs are usually positioned in elevated locations and are typically free from surrounding clutter. However, UEs are most often operated at lower levels and the LOS signal path is often obscured by local obstacles including the user's body itself. Therefore we consider a second type of shadowing which affects (i.e. randomly fluctuates) the dominant signal component. In this contribution, this LOS shadowed small-scale fading is denoted as h and is modeled as a κ-μ shadowed random variable [26], [27]. Together, these two independent random processes create an extremely versatile channel model, $H = h\chi$, which can incorporate a wide range of shadowing and fading scenarios.

1) Large-Scale Shadowing: The analysis presented in this paper is valid for any finite distribution of the large-scale shadowing χ and we summarized the three most commonly used large-scale shadowing distributions, namely the lognormal, gamma, and inverse-Gaussian distributions [30], with the

TABLE I: Special Cases of the κ-μ Shadowed Fading Model.

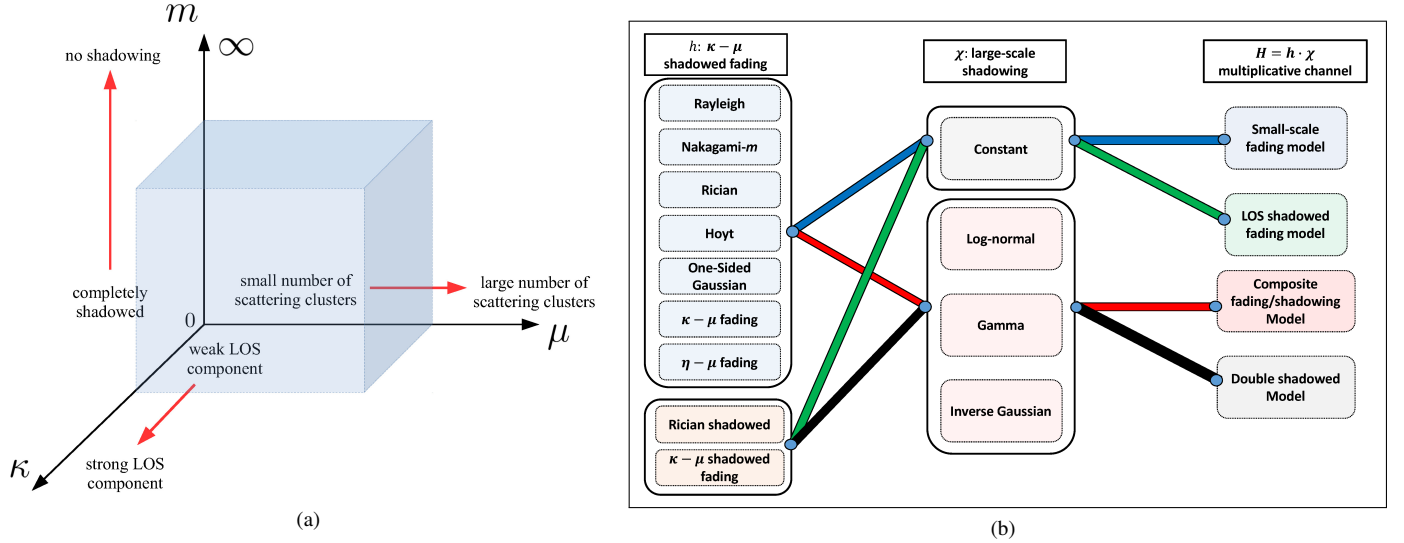|	κ-μ fading	η-μ fading	κ-μ shadowed fading
Rayleigh	$\kappa \to 0, \mu = 1$	$\eta = 1, \mu = 0.5$	$\kappa \to 0, \mu = 1$ or $m = 1, \mu = 1$
Nakagami-m	$\kappa \to 0, \mu = m$	$\eta = 1, \mu = m/2$ or $\eta \to 0, \mu = m$	$\kappa \to 0, \mu = m$ or $m \to m, \mu = m$
Nakagami-n (Rice)	$\mu = 1$		$\kappa = K, \mu = 1, m \to \infty$
Nakagami-q (Hoyt)		$\mu = 0.5$	$\kappa = (1 - q^2)/2q^2, \mu = 1, m = 0.5$
One-sided Gaussian	$\kappa \to 0, \mu = 0.5$	$\eta \to 0, \mu = 0.5$ or $\eta \to \infty, \mu = 0.5$	$\kappa \to 0, \mu = 0.5$ or $m = 0.5, \mu = 0.5$
κ-μ fading	κ, μ		$\kappa \to \kappa, \mu \to \mu, m \to \infty$
η-μ fading		η, μ	$\kappa = (1 - \eta)/2\eta, \mu \to 2\mu, m = \mu$
Rician shadowed			$\kappa = K, \mu = 1, m = m$

Fig. 1: (a) Physical meaning of the channel parameters (κ, μ, m), (b) Versatility of the proposed channel model $H = h \cdot \chi$ with κ-μ shadowed fading h and large-scale shadowing χ.

fractional moment for each distributions below, where l is a positive real number.

(a) Lognormal Shadowing: $\chi \sim LN(\mu_{ln}, \sigma_{ln}^2)$ with mean μ_{ln} and standard deviation σ_{ln},

$$\mathbb{E}\left[\chi^l\right] = \exp\left[\frac{l\mu_{ln}}{\epsilon_0} + \frac{1}{2}\left(\frac{l\sigma_{ln}}{\epsilon_0}\right)^2\right], \quad \epsilon_0 = \frac{10}{\ln(10)}. \quad (5)$$

(b) Gamma Shadowing: $\chi \sim Gamma(k_g, \theta_g)$ with shape parameter k_g and scale parameter θ_g,

$$\mathbb{E}\left[\chi^l\right] = \frac{\Gamma(l + k_g)\theta_g^l}{\Gamma(k_g)}. \quad (6)$$

(c) Inverse Gaussian Shadowing: $\chi \sim IG(\mu_{ig}, \lambda_{ig})$ with mean μ_{ig} and shape parameter λ_{ig},

$$\mathbb{E}\left[\chi^l\right] = e^{\frac{\lambda_{ig}}{\mu_{ig}}} \sqrt{\frac{2\lambda_{ig}}{\pi}} \mu_{ig}^{l-\frac{1}{2}} K_{\frac{1}{2}-l}\left(\frac{\lambda_{ig}}{\mu_{ig}}\right), \quad (7)$$

where $K_n(z)$ is a modified Bessel function of the second kind.

2) Small-Scale Fading and LOS Shadowing: The κ-μ shadowed distribution is a very flexible model which contains as special cases the majority of the linear fading models proposed in the open literature, including Rayleigh, Rice (Nakagami-n), Nakagami-m, Hoyt (Nakagami-q), One-Sided Gaussian, κ-μ, η-μ and Rician shadowed to name a few [31]

(See Table I). Because of this generality, the κ-μ shadowed fading model can be used to account for small-scale fading which originates due to LOS or non-LOS conditions, multipath clustering with circularly symmetric or elliptical scattering, and power imbalance between the in-phase and quadrature signal components.

The channel coefficient h of a κ-μ shadowed fading channel can be expressed in terms of the in-phase and quadrature components of the fading signal as follows

$$h = \sum_{i=1}^{\mu} \left[(X_i + \xi p_i)^2 + (Y_i + \xi q_i)^2\right], \quad (8)$$

where μ is the number of the multipath clusters[4], ξ is a Nakagami-m distributed random variable with $\mathbb{E}\left[\xi^2\right] = 1$, X_i and Y_i are mutually independent Gaussian random variables with

$$\mathbb{E}[X_i] = \mathbb{E}[Y_i] = 0, \quad \mathbb{E}\left[X_i^2\right] = \mathbb{E}\left[Y_i^2\right] = \sigma^2, \quad (9)$$

p_i and q_i are real numbers and $d^2 = \sum_{i=1}^{\mu} \left(p_i^2 + q_i^2\right)$ is the power of the dominant components.

[4]Note that μ is initially assumed to be a natural number, however this restriction is relaxed to allow μ to assume any positive real value.

In the following, we summarize the key statistics of the κ-μ shadowed fading model which will be used in the network performance analysis conducted here.

Lemma 1. *The PDF, fractional moment, and Laplace transform of h for a κ-μ shadowed channel are respectively given by*

$$f_h(x) = \frac{\theta_1^{m-\mu} x^{\mu-1}}{\theta_2^m \Gamma(\mu)} \exp\left(-\frac{x}{\theta_1}\right) {}_1F_1\left[\begin{array}{c} m \\ \mu \end{array}\middle|\, \frac{\theta_2 - \theta_1}{\theta_1 \theta_2} x\right],$$

$$\mathbb{E}\left[h^l\right] = \frac{\theta_1^{m-\mu} \Gamma(\mu+l)}{\theta_2^{m-\mu-l} \Gamma(\mu)} {}_2F_1\left[\begin{array}{c} \mu-m, \mu+l \\ \mu \end{array}\middle|\, -\frac{\mu\kappa}{m}\right], \quad (10)$$

$$\mathcal{L}_h(s) = \mathbb{E}\left[\exp(-sh)\right] = (1+\theta_1 s)^{m-\mu}(1+\theta_2 s)^{-m},$$

where $\bar{h} = \mathbb{E}[h]$, $\theta_1 = \frac{\bar{h}}{\mu(1+\kappa)}$, $\theta_2 = \frac{(\mu\kappa+m)\bar{h}}{\mu(1+\kappa)m}$, κ, μ, m and l are positive real-valued constants, $\Gamma(t)$ is the gamma function and ${}_1F_1\left[\begin{array}{c} a \\ b \end{array}\middle|\, x\right]$ is the confluent hypergeometric function.

Proof. A detailed derivation of the PDF and Laplace transform expression are provided in [26]. The fractional moment of h can be derived as follows

$$\mathbb{E}\left[h^l\right] = \int_0^\infty t^l f_h(t) dt$$

$$= \frac{\theta_1^{m-\mu} \Gamma(\mu+l)}{\theta_2^{m-\mu-l} \Gamma(\mu)} {}_2F_1\left[\begin{array}{c} \mu-m, \mu+l \\ \mu \end{array}\middle|\, -\frac{\mu\kappa}{m}\right], \quad (11)$$

where the PDF $f_h(x)$ from (10) is substituted in the first equality, a change of variables, *i.e.*, $t \leftarrow \frac{\theta_2-\theta_1}{\theta_1\theta_2} x$, and (46) is applied to the last equality. □

Physically, $\kappa = \frac{d^2}{2\mu\sigma^2}$ represents the ratio between the total power of the dominant components and the total power of the scattered waves, μ denotes the real-valued extension of the number of multipath clusters, and m indicates the amount of shadowed perturbation in the dominant component as illustrated in Fig. 1 (a). Since the Laplace transform of the Nakagami-m distribution converges to $\lim_{m\to\infty} \mathcal{L}_h(s) = \lim_{m\to\infty}(1+s\bar{h}/m)^{-m} = e^{-s\bar{h}}$, the dominant component becomes increasingly deterministic as $m \to \infty$. Hence, a κ-μ shadowed fading channel where $m \to \infty$ has a constant dominant power and is therefore equivalent to a κ-μ faded channel.

3) Combined Large-Scale Shadowing, Small-Scale Fading and LOS Shadowing: Since the κ-μ shadowed fading model includes small-scale fading and LOS shadowed fading as special cases, the proposed channel model $H = h\chi$ can be used to represent four different classes of fading environment as illustrated in Fig. 1 (b); namely 1) small-scale fading only if χ is constant, 2) small-scale fading with LOS shadowed fading only if h is either Rician shadowed or κ-μ shadowed and χ is constant, 3) traditional composite fading/shadowing if h is the result of small-scale fading only with randomly distributed χ, and 4) double shadowed fading conditions if h is the result of small-scale and LOS shadowed fading and χ is a random variable.

Remark 1. *Multiple Antenna Systems: If the BS is equipped with N_c antennas and communicating with a single-antenna UE with zero-force beamforming, the corresponding channel* between the BS and a UE can be represented as a summation of N_c i.i.d. κ-μ shadowed random variables, which is a κ-μ shadowed random variable with fading parameters $(\kappa, N_c\mu, N_c m)$ [26], [31]. Thereby, the theoretical analysis presented in this paper can be directly applied to multiple-antenna diversity systems.

III. LAGUERRE POLYNOMIAL SERIES EXPANSION OF THE κ-μ SHADOWED DISTRIBUTION

As we can see from (10), the κ-μ shadowed distribution includes the hypergeometric function which often leads to a computationally complex performance evaluation. Due to the inherent mathematical intractability, limited work has been conducted which considers κ-μ shadowed fading in the context of stochastic geometry. Most notably, in [32], the author approximated a κ-μ shadowed random variable using a gamma distributed random variable based on second-order moment matching, but the accuracy of this approximation can not be guaranteed for all fading parameters. In [33], the authors analyzed a cellular network over κ-μ shadowed fading where they represented the confluent hypergeometric function by its truncated series form, *i.e.*, ${}_1F_1\left[\begin{array}{c} a \\ b \end{array}\middle|\, x\right] \simeq \sum_{n=0}^N \frac{\Gamma(a+n)\Gamma(b)x^n}{\Gamma(a)\Gamma(b+n)n!}$. Although the series representation converges locally, it is valid only for integer-valued parameters a and b, the radius of convergence diverges over different combinations of parameters, and is computationally complex to evaluate. As illustrated in Fig. 2, there are noticeable discrepancies between the approximation methods proposed in [32] and [33] and the exact PDF for several cases, limiting their application[5].

To overcome this problem, we adopt the generalized Laguerre polynomial expansion proposed in [34], [35] that is analogous to the Fourier series: As a Fourier series can represent any PDF in terms of harmonic bases, we use a generalized Laguerre polynomial as an orthogonal base and simplify the PDF and CDF of the κ-μ shadowed fading model as given below.

Lemma 2. *The PDF and CDF of the channel coefficient h for the κ-μ shadowed fading model can be expressed in series expression form as follows*

$$f_h(x) = \sum_{n=0}^\infty \frac{n! C_n L_n^{\mu-1}(x)}{\Gamma(n+\mu)} x^{\mu-1} \exp(-x)$$

$$= \sum_{n=0}^\infty \sum_{i=0}^n c_{i,n}\, x^{\mu+i-1} \exp(-x), \quad (12)$$

$$F_h(x) = \int_0^x f_h(t) dt$$

$$= \sum_{n=0}^\infty \sum_{i=0}^n b_{i,n}\, x^{\mu+i} \exp(-x) + \frac{\gamma(\mu, x)}{\Gamma(\mu)}, \quad (13)$$

where κ, μ and m are positive real-valued parameters, $L_n^{\mu-1}(x)$ is the generalized Laguerre polynomial of degree n and order $\mu-1$ at x, $0 \le x < \infty$, $\gamma(\mu, x)$ is the lower incomplete gamma

[5]The approximation accuracy of [33] depends on N. For a larger N, [33] may accurately approximate the exact PDF. In contrast, the proposed approach in (12) converges rapidly to the exact PDF even with a small number of terms $N \le 50$.
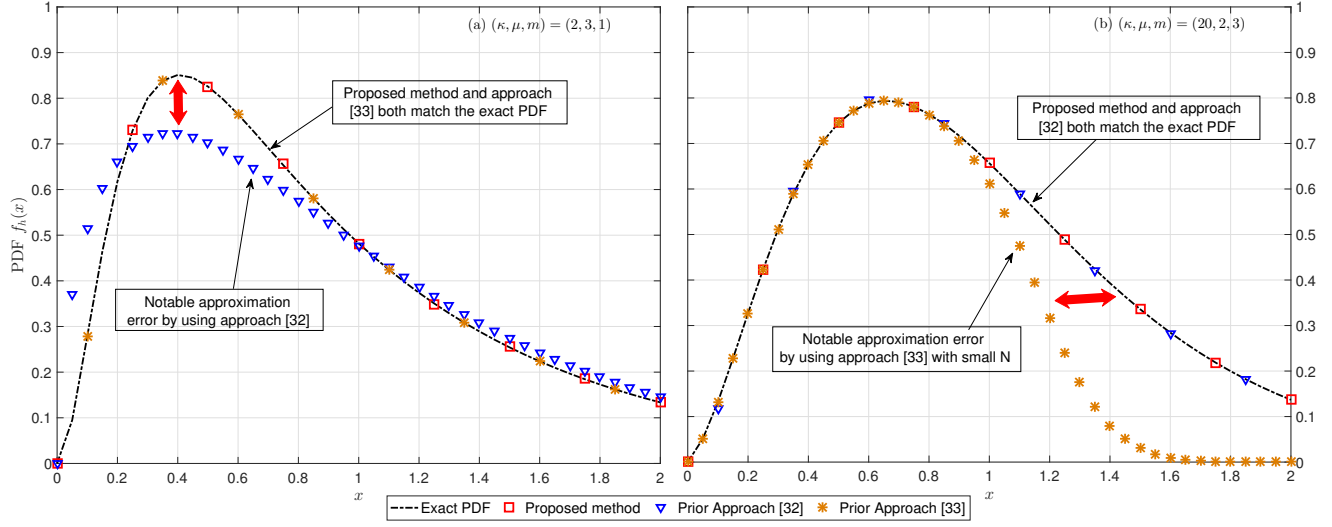
Fig. 2: Numerical evaluation of the κ-μ shadowed fading distribution using the PDFs given in (10), (12), [32], and [33]; (a) $(\kappa, \mu, m) = (2, 3, 1)$ and (b) $(\kappa, \mu, m) = (20, 2, 3)$ case, respectively.

function, the coefficients C_n, $c_{i,n}$, and $b_{i,n}$ are calculated as written below

$$C_n = \sum_{j=0}^{n} \frac{(-1)^j}{j!} \binom{n+\mu-1}{n-j} \mathbb{E}\left[h^j\right],$$

$$c_{i,n} = \frac{(-1)^i C_n}{\Gamma(\mu+i)} \binom{n}{i}, \quad b_{i,n} = \frac{(-1)^i C_{n+1}}{\Gamma(\mu+i+1)} \binom{n}{i}, \quad (14)$$

and $\mathbb{E}\left[h^j\right]$ can be obtained from (11) by substituting non-negative integer index j to the index l.

Proof. See Appendix II. □

Remark 2. *If μ and m are positive integers, then by using [36, Theorem 1], the expression in (12) can be simplified to a single summation with finite terms as follows.*

$$f_h(x) = \begin{cases} \sum_{j=1}^{\mu-m} \frac{A_{1j} x^{\mu-m-j} e^{-\frac{x}{\theta_1}}}{\Gamma(\mu-m-j+1)\theta_1^{\mu-m-j+1}} \\ \quad + \sum_{j=1}^{m} \frac{A_{2j} x^{m-j} e^{-\frac{x}{\theta_2}}}{\Gamma(m-j+1)\theta_2^{m-j+1}} \quad \text{for } m < \mu, \quad (15) \\ \sum_{j=0}^{m-\mu} \frac{B_j x^{m-j-1} e^{-\frac{x}{\theta_2}}}{\Gamma(m-j)\theta_2^{m-j}} \quad \text{for } m \geq \mu \end{cases}$$

where A_{1j}, A_{2j}, B_j are given in [36, eq (6)]. (12) and (15) imply that κ-μ shadowed fading is the result of a linear combination of Gamma distributed random variables, which follows a gamma mixture distribution. To represent κ-μ shadowed fading as a gamma mixture model, a double summation with infinite terms are required for real valued μ and m, whereas for integer valued μ and m, only a single summation with finite terms are necessary.

IV. DISTRIBUTION OF THE AGGREGATE INTERFERENCE

In this section, we calculate the Laplace transform of the aggregate interference for the κ-μ shadowed fading channel

and characterize the distribution of the interference. As shall be seen in Section V, the Laplace transform of the aggregate interference is a crucial measure for evaluating network performance in stochastic geometry based analyses.

Lemma 3. *Given that a typical UE is associated to the BS y_k^* located at $\|y_k^*\| = r$ (or equivalently expressed as x_k^* using $x = \chi_j^{\frac{1}{\alpha}} y$), the Laplace transform of the aggregate interference over a multiplicative channel with κ-μ shadowed fading and large-scale shadowing is calculated as*

$$\mathcal{L}_I(s) = \mathbb{E}\left[\exp(-sI)\right]$$

$$= \mathbb{E}\left[\exp\left(-s \sum_{j \in \mathcal{K}} \sum_{y \in \Phi_j^{(e)} \setminus \{y_k^*\}} \hat{P}_j h_y \|y\|^{-\alpha}\right)\right] \quad (16)$$

$$= \exp\left[-\sum_{j \in \mathcal{K}} \pi r^2 \lambda_j \mathbb{E}\left[\chi_j^\delta\right] \hat{P}_j^\delta \hat{B}_j^\delta \mathcal{W}_j(z)\right],$$

where the subindex $j \in \mathcal{K} = \{1, 2, \ldots, K\}$ represents the parameters for the j-th tier, $\hat{P}_j = \frac{P_j}{P_k}$, $\mathbb{E}\left[\chi_j^\delta\right]$ is given by (5)-(7), $\mathcal{W}_j(z)$ denotes the following expression

$$\mathcal{W}_j(z) = \frac{\mu \theta_1 z}{1-\delta} \left(\frac{\theta_1}{\theta_2}\right)^m \frac{F_2(\mu+1; m, 1; \mu, 2-\delta; A, B)}{(1+\theta_1 z)^{\mu+1}}$$

$$- \left[1 - \frac{(1+\theta_1 z)^{m-\mu}}{(1+\theta_2 z)^m}\right], \quad (17)$$

for $z = sr^{-\alpha}$, $A = \frac{1-\theta_1/\theta_2}{1+\theta_1 z}$, $B = \frac{\theta_1 z}{1+\theta_1 z}$, $\theta_1 = \frac{\bar{h}}{\mu(1+\kappa)}$ and $\theta_2 = \frac{(\mu\kappa+m)\bar{h}}{\mu(1+\kappa)m}$. $F_2(\cdot)$ is the Appell Hypergeometric function which is defined in (53), Appendix I [37].

Proof. See Appendix III. Some comments on the numerical computation of the Appell's function $F_2(\cdot)$ are presented in Appendix IV. □

By using a change of variable, *i.e.*, $sz^{-1} = r^\alpha$, the Laplace transform of the interference can be expressed as

$$\mathcal{L}_I(s) = \exp\left[-\sum_{j \in \mathcal{K}} \pi \lambda_j \mathbb{E}\left[\chi_j^\delta\right]\left(\hat{P}_j z^{-1}\right)^\delta \mathcal{W}_j(z) s^\delta\right],$$

which indicates that the aggregate interference is distributed by a Stable distribution as described below. Note that the exclusion zone in the interference field is considered in (16) based on the condition $\|y_k^*\| = r$.

Lemma 4. *The aggregate interference over a multiplicative channel of κ-μ shadowed fading and large-scale shadowing is distributed by a Stable distribution [3] with four parameters; namely, stability δ, skew = 1, drift = 0, dispersion = $\sec\left(\frac{\pi}{2}\delta\right) \sum_{j \in \mathcal{K}} \pi \lambda_j \mathbb{E}\left[\chi_j^\delta\right] \hat{P}_j^\delta \hat{B}_j^\delta z^{-\delta} \mathcal{W}_j(z)$ with $\mathcal{W}_j(z)$ defined in (17). The fractional moment of the aggregate interference is given by*

$$\mathbb{E}\left[I^l\right] = \frac{\Gamma\left(1 - \frac{l}{\delta}\right)}{\Gamma(1-l)\cos\left(\frac{\pi}{2}\delta\right)^{\frac{l}{\delta}}}\left[\sum_{j \in \mathcal{K}} \pi r^2 \lambda_j \mathbb{E}\left[\chi_j^\delta\right] z_j^{-\delta} \mathcal{W}(z_j)\right]^{\frac{\delta}{l}},$$

(18)

for $0 < l < \frac{2}{\alpha}$. Any moment with order above $l > \frac{2}{\alpha}$ is undefined, i.e., becomes infinity.

Using (54), the Appell's function reduces to a Gauss hypergeometric function if one of the parameters is zero. Hence the expressions in (16) and (17) can be simplified as below.

Lemma 5. *For the following fading distributions, $\mathcal{W}_j(z)$ in (17) can be simplified as follows*
Rayleigh:

$$\frac{\bar{h}\delta z}{1-\delta} \,_2F_1\left[\begin{matrix}1, 1-\delta\\2-\delta\end{matrix} \middle| -\bar{h}z\right]$$

(19)

Nakagami-m:

$$\frac{\bar{h}z}{1-\delta} \,_2F_1\left[\begin{matrix}m+1, 1-\delta\\2-\delta\end{matrix} \middle| -\frac{\bar{h}z}{m}\right] - \left[1 + \left(1 + \frac{\bar{h}z}{m}\right)^{-m}\right]$$

(20)

One-Sided Gaussian:

$$\frac{\bar{h}z}{1-\delta} \,_2F_1\left[\begin{matrix}1.5, 1-\delta\\2-\delta\end{matrix} \middle| -2\bar{h}z\right] - \left[1 - \frac{1}{\sqrt{1+2\bar{h}z}}\right]$$

(21)

κ-μ fading:

$$\frac{\mu\theta_1 z}{(1-\delta)e^{\mu\kappa}} \,_2F_1\left[\begin{matrix}\mu+1, 1-\delta\\2-\delta\end{matrix} \middle| -\theta_1 z\right] - \left[1 - \frac{e^{-\frac{\mu\kappa}{1+(\theta_1 z)^{-1}}}}{(1+\theta_1 z)^\mu}\right]$$

(22)

Rician:

$$\frac{\theta_1 z}{(1-\delta)e^K} \,_2F_1\left[\begin{matrix}2, 1-\delta\\2-\delta\end{matrix} \middle| -\theta_1 z\right] - \left[1 - \frac{e^{-\frac{K}{1+(\theta_1 z)^{-1}}}}{1+\theta_1 z}\right]$$

(23)

Proof. See Appendix V. □

V. THEORETICAL ANALYSIS OF THE PERFORMANCE MEASURES

In this section, we propose a novel method to compute $\mathbb{E}[g(\gamma)]$ for an arbitrary function of the SINR $g(\gamma)$ using stochastic geometry. The original idea was proposed by Hamdi in [38] for Nakagami-m fading, and later in [39] for κ-μ and η-μ fading, which we further extend it to κ-μ shadowed fading in this paper. By using the proposed method, one can evaluate any performance measures that are represented as a function of SINR (or SIR). For instance, the spectral efficiency, outage probability, moments of the SINR, and error probability can be expressed as an average of $g(x) = \log(1+x)$, $g(x) = \mathbb{I}(x \le x_0)$, $g(x) = x^n$, and $g(x) = Q(x)$, respectively.

A. General Case and Main Result

Theorem 1. *For the K-tier HetNet with κ-μ shadowed fading, $\mathbb{E}[g(\text{SINR})]$ is given by*

$$\mathbb{E}[g(\text{SINR})] = \sum_{k=1}^{K} \mathcal{P}_k \mathbb{E}[g(\text{SINR}_k)],$$

$$\mathbb{E}[g(\text{SINR}_k)] = \sum_{n=0}^{\infty} C_n \sum_{i=0}^{n}(-1)^i \binom{n}{i}\xi_i,$$

(24)

where $\mathcal{P}_k$ is derived in (4), SINR_k represents the SINR when a typical UE is associated to the k-th tier BS y_k^*, C_n is defined in (14), and ξ_i represents the following integral

$$\xi_i \triangleq \int_0^\infty g_{\mu+i}(z)\, \mathbb{E}_r\left[e^{-r^\alpha \hat{N}z}\mathcal{L}_I(r^\alpha z)\right]\mathrm{d}z,$$

(25)

the distribution $f_{\|y_k^*\|}(r)$ is given by (4) and $\mathcal{L}_I(s)$ is derived in (16). $g_{\mu+i}(z)$ is defined as

$$g_{\mu+i}(z) = \frac{1}{\Gamma(\mu+i)}\frac{\mathrm{d}^{\mu+i}}{\mathrm{d}z^{\mu+i}}z^{\mu+i-1}g(z)$$

$$= \sum_{n=0}^{\mu+i-1}\binom{\mu+i}{n}\frac{z^{\mu+i-1-n}}{\Gamma(\mu+i-n)}\frac{\mathrm{d}^{\mu+i-n}}{\mathrm{d}x^{\mu+i-n}}g(z),$$

(26)

where we used the general Leibniz rule in the last equality.

Proof. See Appendix VI. □

Theorem 1 is the most general result in this paper that evaluates arbitrary performance measures for a K-tier HetNet, considering noise, interference, per-tier BS density, and independent fading and shadowing across each tier. The analytic function $g(z)$ and $g_{\mu+i}(z)$ for various performance measure are summarized in Table II[6]. We also note that $\mathbb{E}[g(\text{SINR}_k)]$ in (24) is computationally efficient; the computational complexity of (24) is same as a single summation expression since ξ_i is independent of the index n.

Remark 3. *If μ and m are positive integers, (15) can be utilized to achieve an expression analogous to Theorem 1, in*

---

[6]The detailed proof of Table II is given in [38], [39].

TABLE II: Theoretical framework for evaluating various system measures.

$g(x)$ and $g_{\mu+i}(x)$ for various system measures		
Measure	$g(x)$	$g_{\mu+i}(x) = \frac{1}{\Gamma(\mu+i)}\frac{\mathrm{d}^{\mu+i}}{\mathrm{d}z^{\mu+i}}x^{\mu+i-1}g(x)$
Rate	$\log(1+x)$	$\frac{1}{x}\left(1 - \frac{1}{(1+x)^{\mu+i}}\right)$
Higher order moments	x^l	$\frac{\Gamma(\mu+i+l)}{\Gamma(\mu+i)\Gamma(l)}x^{l-1}$
Outage probability	$\mathbb{I}(x \le x_0) \simeq \frac{1}{1+e^{-\epsilon(x-x_0)}}$	$\sum_{k=0}^{\mu+i-1}\binom{\mu+i}{k}\frac{z^{\mu+i-1-k}}{\Gamma(\mu+i-k)}\frac{\mathrm{d}^{\mu+i-k}}{\mathrm{d}x^{\mu+i-k}}\mathbb{I}(x \le x_0)$
$\mathbb{E}_r\left[e^{-r^\alpha \hat{N}z}\mathcal{L}_I(r^\alpha z)\right]$ for various scenarios		
$\alpha = 4$, i.i.d. fading	$\frac{\sqrt{\pi}\Theta}{1+\mathcal{W}(z)}\exp\left(\Theta^2\right)\mathrm{erfc}(\Theta), \qquad \Theta = \frac{\pi\lambda_0}{2\sqrt{\hat{N}z}}(1+\mathcal{W}(z))$	
Interference-limited, i.i.d. fading	$\frac{1}{1+\mathcal{W}(z)}$	
Noise-limited, i.i.d. fading	$\sqrt{\pi}\Theta\exp\left(\Theta^2\right)\mathrm{erfc}(\Theta), \qquad \Theta = \frac{\pi\lambda_0}{2\sqrt{\hat{N}z}}$	
Main result		
κ-μ shadowed fading	$\mathbb{E}[g(\mathrm{SINR}_k)] = \sum_{n=0}^{\infty}C_n\sum_{i=0}^{n}(-1)^i\binom{n}{i}\int_0^\infty g_{\mu+i}(z)\mathbb{E}\left[e^{-r^\alpha \hat{N}z}\mathcal{L}_I(r^\alpha z)\right]\mathrm{d}z$	
Rayleigh fading	$\mathbb{E}[g(\mathrm{SINR}_k)] = \int_0^\infty \frac{\partial g(z)}{\partial z}\mathbb{E}\left[e^{-r^\alpha \hat{N}z}\mathcal{L}_I(r^\alpha z)\right]\mathrm{d}z$	

terms of a single summation with finite terms as described below

$$\mathbb{E}[g(\mathrm{SINR}_k)] = \begin{cases} \sum_{j=1}^{\mu-m}A_{1j}\zeta_{\mu-m-j+1}(\theta_1) \\ \quad + \sum_{j=1}^{m}A_{2j}\zeta_{m-j+1}(\theta_2) & \textit{for } m < \mu , \quad (27) \\ \sum_{j=0}^{m-\mu}B_j\zeta_{m-j}(\theta_2) & \textit{for } m \ge \mu \end{cases}$$

where $\zeta_j(\theta) = \int_0^\infty g_j(z)\,\mathbb{E}_r\left[e^{-\frac{r^\alpha}{\theta}\hat{N}z}\mathcal{L}_I\left(\frac{r^\alpha}{\theta}z\right)\right]\mathrm{d}z$ and the coefficients A_{1j}, A_{2j}, B_j are derived in [36, eq (6)]. The proof of (27) is omitted since it is analogous to Theorem 1.

B. Special Cases

Theorem 1 and $\mathbb{E}_r\left[e^{-r^\alpha \hat{N}z}\mathcal{L}_I(r^\alpha z)\right]$ can be further simplified for some special cases, such as a noise-limited scenario, an interference-limited scenario, or identical fading and shadowing parameters on all tiers, which are described below.

Lemma 6. *Fixed path-loss* ($\alpha = 4$): *If $\alpha = 4$, the term $\mathbb{E}_r\left[e^{-r^4\hat{N}z}\mathcal{L}_I(r^4z)\right]$ in (25) can be simplified as*

$$\frac{\pi^{\frac{3}{2}}\sum_{j\in\mathcal{K}}\lambda_j\mathbb{E}\left[\chi_j^{\frac{1}{2}}\right]\hat{P}_j^{\frac{1}{2}}\hat{B}_j^{\frac{1}{2}}}{2\sqrt{\hat{N}z}}\exp\left(\Theta^2\right)\mathrm{erfc}(\Theta), \qquad (28)$$

where Θ denotes the following expression

$$\Theta \triangleq \frac{\pi}{2\sqrt{\hat{N}z}}\sum_{j\in\mathcal{K}}\left(\lambda_j\mathbb{E}\left[\chi_j^{\frac{1}{2}}\right]\hat{P}_j^{\frac{1}{2}}\hat{B}_j^{\frac{1}{2}}(1+\mathcal{W}_j(z))\right),$$

*and $\mathcal{W}_j(z)$ is defined in (17). If all tiers have **identical fading parameters** (κ, μ, m), then $\mathcal{W}(z) = \mathcal{W}_j(z)$ for any $j \in \mathcal{K}$ and (28) can be further simplified as*

$$\Theta = \frac{\pi\lambda_0}{2\sqrt{\hat{N}z}}(1+\mathcal{W}(z)), \quad \lambda_0 \triangleq \sum_{j\in\mathcal{K}}\lambda_j\mathbb{E}\left[\chi_j^{\frac{1}{2}}\right]\hat{P}_j^{\frac{1}{2}}\hat{B}_j^{\frac{1}{2}},$$

$$\mathbb{E}_r\left[e^{-r^4\hat{N}z}\mathcal{L}_I(r^4z)\right] = \frac{\sqrt{\pi}\Theta}{1+\mathcal{W}(z)}\exp\left(\Theta^2\right)\mathrm{erfc}(\Theta). \qquad (29)$$

Lemma 7. *Interference-limited scenario*: *If $I \gg \hat{N}$, the term $\mathbb{E}_r\left[e^{-r^\alpha \hat{N}z}\mathcal{L}_I(r^\alpha z)\right]$ in (25) can be simplified as*

$$\frac{\sum_{j\in\mathcal{K}}\lambda_j\mathbb{E}\left[\chi_j^\delta\right]\hat{P}_j^\delta\hat{B}_j^\delta}{\sum_{j\in\mathcal{K}}\lambda_j\mathbb{E}\left[\chi_j^\delta\right]\hat{P}_j^\delta\hat{B}_j^\delta(1+\mathcal{W}_j(z))}. \qquad (30)$$

*If all tiers have **identical fading characteristics**, then (30) reduces to a succinct form as*

$$\mathbb{E}_r\left[e^{-r^\alpha \hat{N}z}\mathcal{L}_I(r^\alpha z)\right] = [1+\mathcal{W}(z)]^{-1}. \qquad (31)$$

Lemma 8. *Noise-limited scenario with fixed path-loss* ($\alpha = 4$): *If $I \ll \hat{N}$ and $\alpha = 4$, then $\mathbb{E}_r\left[e^{-r^4\hat{N}z}\mathcal{L}_I(r^4z)\right]$ can be simplified as*

$$\sqrt{\pi}\Theta\exp\left(\left(\frac{\pi\lambda_0}{2\sqrt{\hat{N}z}}\right)^2\right)\mathrm{erfc}\left(\frac{\pi\lambda_0}{2\sqrt{\hat{N}z}}\right). \qquad (32)$$

Proof. The proof of Lemmas 6, 7 and 8 are given in Appendix VII. □

Remark 4. *If all tiers have identical fading characteristics and are interference-limited only, the performance measure $\mathbb{E}[g(\mathrm{SINR})]$ can be expressed by using Lemma 5 as follows*

$$\mathbb{E}[g(\mathrm{SINR})] = \sum_{n=0}^{\infty}C_n\sum_{i=0}^{n}(-1)^i\binom{n}{i}\int_0^\infty\frac{g_{\mu+i}(z)}{1+\mathcal{W}(z)}\mathrm{d}z, \quad (33)$$

where C_n, $g_{\mu+i}(z)$ and $\mathcal{W}(z)$ are independent of the PPP density λ_j. (33) provides an important insight into the system performance of a PPP-distributed cellular network with κ-μ shadowed fading and arbitrary large-scale shadowing. Specifically, any performance measure of a PPP-distributed HetNet that can be represented as a function of SINR, is independent to the BS transmit power P_k, BS density λ_k, and the number of tiers K. This invariance property was originally introduced in [6], [7], [9] for Rayleigh fading. (33) generalizes this argument by proving that the invariance property holds for any linear small-scale fading and finite large-scale shadowing distribution.

Next, we apply Theorem 1, Lemmas $5, 6$ and 7 to evaluate various performance measures.

C. Performance Measure 1: Spectral Efficiency

Spectral efficiency is defined in [7] as

$$\mathcal{R} = \sum_{k=1}^{K} \mathcal{P}_k \, \mathbb{E}\left[\ln\left(1 + \text{SINR}_k\right)\right],$$

where $\mathcal{P}_k$ is the tier association probability to the k-th tier evaluated by (3) and SINR_k is the received SINR from the k-th tier BS. $\mathbb{E}\left[\ln\left(1 + \text{SINR}_k\right)\right]$ can be evaluated by using Theorem 1 with $g(z) = \ln(1+z)$ and $g_{\mu+i}(z)$ as follows [38]

$$
\begin{aligned}
g_{\mu+i}(z) &= \frac{1}{\Gamma(\mu+i)} \frac{d^{\mu+i}}{dz^{\mu+i}} z^{\mu+i-1} g(z) \\
&= \frac{1}{z}\left(1 - \frac{1}{(1+z)^{\mu+i}}\right).
\end{aligned}
\tag{34}
$$

Given identical channel characteristics across each tier, the spectral efficiency reduces to

$$
\begin{aligned}
\mathcal{R} &= \mathbb{E}\left[\ln\left(1 + \text{SINR}_k\right)\right] \\
&= \sum_{n=0}^{\infty} C_n \sum_{i=0}^{n} (-1)^i \binom{n}{i} \int_0^\infty \frac{\mathcal{K}(z)}{z}\left(1 - \frac{1}{(1+z)^{\mu+i}}\right) dz,
\end{aligned}
\tag{35}
$$

where C_n is given by (12), $\mathcal{W}(z)$ is derived in (17), Θ is defined in (28) and $\mathcal{K}(z)$ denotes

$$
\mathcal{K}(z) =
\begin{cases}
\dfrac{\sqrt{\pi}\Theta}{1 + \mathcal{W}(z)} \exp\left(\Theta^2\right) \text{erfc}\left(\Theta\right) & \text{for } \alpha = 4, \\[3mm]
\dfrac{1}{1 + \mathcal{W}(z)} & \text{for } I \gg \hat{N}
\end{cases}.
\tag{36}
$$

Remark 5. *Theorem 1 can be applied to Rayleigh fading by letting $\mu = 1.0$, $C_0 = 1$ and $C_n = 0$ for $n > 0$ in (24). Then (35) can be further simplified as follows*

$$
\begin{aligned}
\mathcal{R} &= \int_0^\infty \frac{1}{(1+z)(1+\mathcal{W}(z))} dz \\
&= \int_0^\infty \frac{1}{(1+\mathcal{W}(e^t - 1))} dt,
\end{aligned}
\tag{37}
$$

by using a change of variable, i.e., $x = e^t - 1$. As expected, the above expression is identical to [7, Eq.(27)].

D. Performance Measure 2: Moments of the SINR

Higher order moments of the SINR are a crucial performance measure which have an important role in the determination of network performance. $\mathbb{E}\left[\text{SINR}^l\right]$ can be evaluated by using Theorem 1 with $g(z) = z^l$ and $g_{\mu+i}(z)$ as

$$
g_{\mu+i}(z) = \frac{1}{\Gamma(\mu+i)} \frac{d^{\mu+i}}{dz^{\mu+i}} z^{\mu+i-1} g(z) = \frac{\Gamma(\mu+i+l)}{\Gamma(l)\Gamma(\mu+i)} z^{l-1}.
\tag{38}
$$

For the case when we have identical channel characteristics across each tier, the fractional moment is simplified to

$$
\mathbb{E}\left[\text{SINR}^l\right] = \sum_{n=0}^{\infty} C_n \sum_{i=0}^{n} (-1)^i \binom{n}{i} \frac{(\mu+i)_l}{\Gamma(l)} \int_0^\infty z^{l-1} \mathcal{K}(z) dz,
\tag{39}
$$

where $(x)_n = \frac{\Gamma(x+n)}{\Gamma(x)}$ is the Pochhammer symbol, the index l is a positive real-valued constant and $\mathcal{K}(z)$ is defined in (36).

E. Performance Measure 3: Outage Probability

The outage probability is defined in [6] as

$$
P_o(T) = \mathbb{P}\left(\text{SINR} < T\right) = \sum_{k=1}^{K} \mathcal{P}_k \mathbb{P}\left(\text{SINR}_k < T\right),
\tag{40}
$$

for a predefined threshold T. Theoretically, one can use Theorem 1 to calculate (40) by approximating the step function with a smooth sigmoid function, *i.e.*, $g(z) = \mathbb{I}(z < T_o) \simeq \frac{1}{1 + e^{-\epsilon(z-T_o)}}$, where ϵ controls the sharpness. However, even with a smooth function, $g_{\mu+i}(z)$ behaves like an impulse signal for a large derivation order $\mu + i$ [40]. Hence, most numerical software will present a precision overflow while evaluating (25).

Instead of using Theorem 1, it appears more convenient to use the Gil-Pelaez's inversion based approach [41] as follows. **Step 1)** $\mathbb{P}\left(\text{SINR}_k < T\right)$ in (40) can be represented in terms of the interference distribution as follows

$$
\begin{aligned}
\mathbb{P}\left(\text{SINR}_k < T\right) &= 1 - \mathbb{E}\left[\mathbb{P}\left(h_{y_k^*} r^{-\alpha} > T(I + \hat{N})\right)\right] \\
&= 1 - \mathbb{E}\left[\mathbb{P}\left(I < \frac{h_{y_k^*} r^{-\alpha}}{T} - \hat{N}\right)\right],
\end{aligned}
\tag{41}
$$

where the expectation in (41) average over the link length r and the channel coefficient h. **Step 2)** The CDF of the interference can be derived using the Gil-Pelaez's inversion as follows

$$
\mathbb{P}\left(I < x\right) = \frac{1}{2} + \frac{1}{\pi} \int_0^\infty \frac{Im\{e^{itx} \mathcal{L}_I(it)\}}{2t} dt, \quad i = \sqrt{-1},
\tag{42}
$$

where $Im(z)$ represents the imaginary part of a complex number z. **Step 3)** (41) can be further simplified if each tier has identical fading parameters as follows

$$
\begin{aligned}
\mathbb{P}\left(I < x\right) &= \frac{1}{2} + \int_0^\infty Im\left\{\frac{\left(1 + \frac{i\theta_1 x}{T}\right)^{m-\mu}}{\left(1 + \frac{i\theta_2 x}{T}\right)^{m}} \phi(x)\right\} \frac{dx}{x}, \\
\phi(x) &\triangleq \int_0^\infty \exp\left[i\hat{N}\lambda_0^{-\frac{1}{\delta}} x t^{\frac{1}{\delta}} - \pi t \varphi(ix)\right] dt, \\
\varphi(z) &= \mathbb{E}_h\left[{}_1F_1\left[\begin{array}{c} -\delta \\ 1-\delta \end{array}\middle| zh\right]\right],
\end{aligned}
\tag{43}
$$

where we applied [41, Eq. 4] to (41) and (42). If the noise can be neglected, *i.e.*, $\hat{N} \to 0$, then $\phi(x) = \frac{1}{\pi\varphi(ix)}$ and $\mathbb{P}\left(\text{SINR}_k < T\right)$ can be simplified as follows

$$
\frac{1}{2} + \frac{1}{\pi} \int_0^\infty \frac{Im\left\{\left(1 + \frac{i\theta_1 x}{T}\right)^{m-\mu}\left(1 + \frac{i\theta_2 x}{T}\right)^{-m}\right\}}{x\varphi(ix)} dx.
\tag{44}
$$

VI. Numerical Results

In this section, we present numerical evaluations of the theoretical results and compare them with Monte-Carlo simulations. All of the numerical results presented in this paper were obtained by using the Julia language which provides fast computation times and a straight-forward syntax that is similar to Matlab [42]. The analytical results are plotted as lined curves without markers, whereas the simulation results are represented by markers without a line. Both Fig. 3 and 4 show that the numerical results accurately match the simulation results in every scenario. In our analysis, we considered a
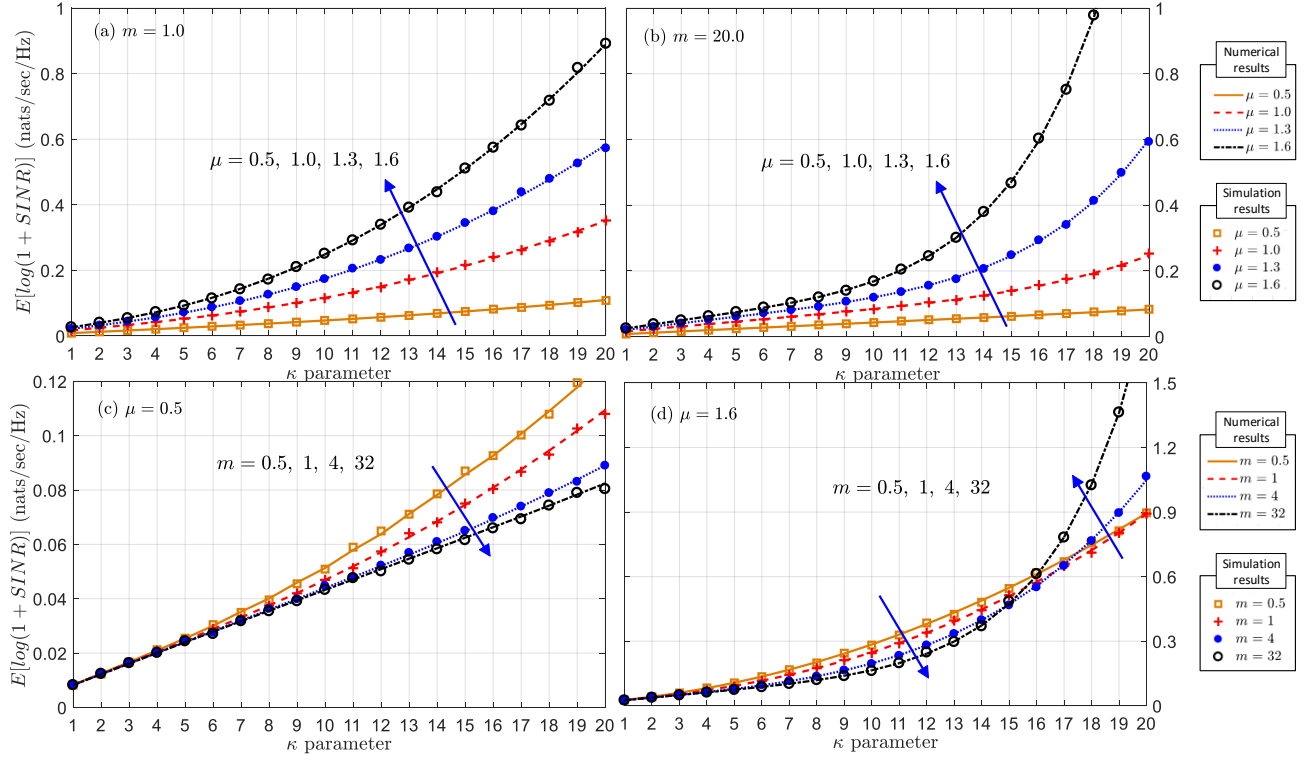
Fig. 3: Spectral efficiency of a two-tier HetNet over various channel parameters assuming interference-limited scenario environment with $\lambda_1 = \frac{1}{\pi 500^2}$, $P_1 = 53$ dBm, $\bar{h} = 1$; (a) $m = 1.0$, (b) $m = 20.0$, (c) $\mu = 0.5$ and (d) $\mu = 1.6$ case, respectively.
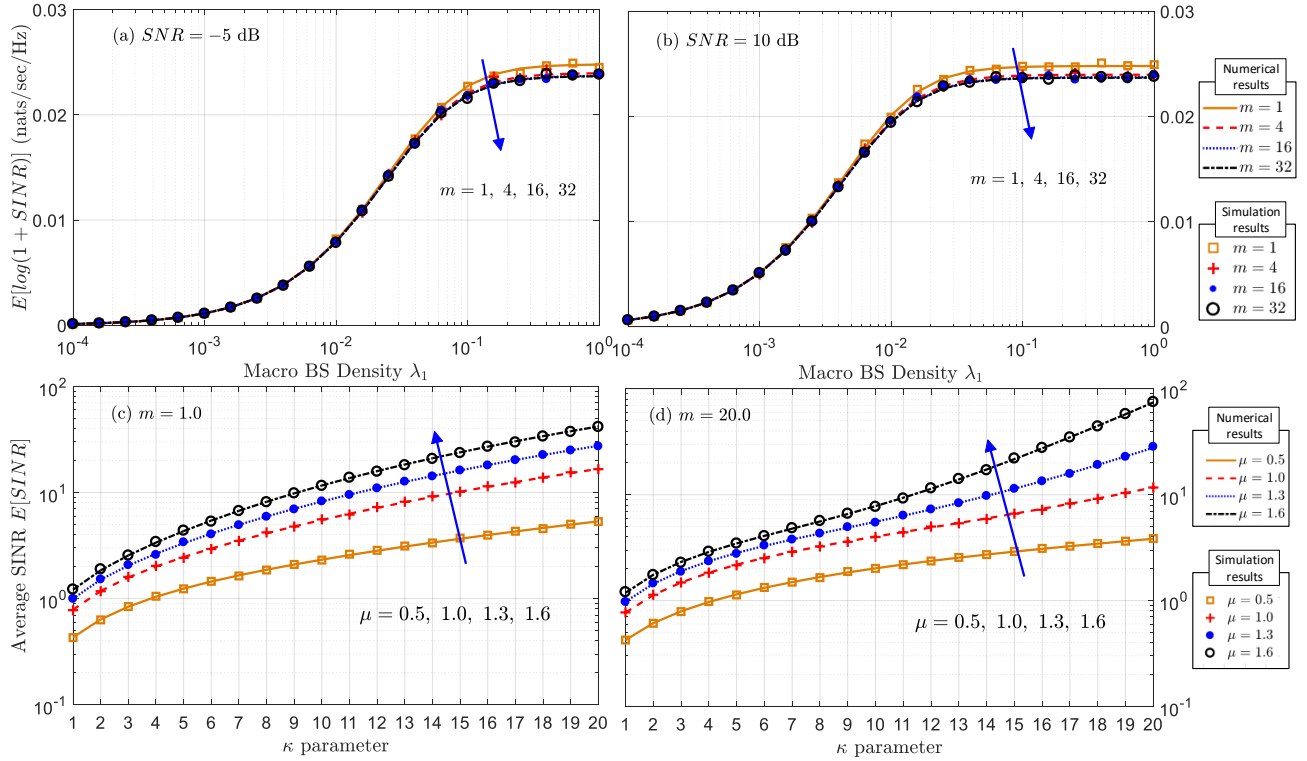

Fig. 4: Spectral efficiency and average SINR of a two-tier HetNet over various channel parameters with $P_1 = 53$ dBm, $\bar{h} = 1$; (a) $\kappa = 2$, $\mu = 1$, $SNR = -5$ dB, (b) $\kappa = 2$, $\mu = 1$, $SNR = 10$ dB, (c) $m = 1$, $\lambda_1 = \frac{1}{\pi 500^2}$, $\hat{N} \to 0$ and (d) $m = 20$, $\lambda_1 = \frac{1}{\pi 500^2}$ and $\hat{N} \to 0$, respectively.

two-tier HetNet with BS intensity $\lambda_1 = 2\lambda_2$, transmit power $P_2 = P_1 - 20$ dBm, a path-loss exponent $\alpha = 4$ and lognormal distributed χ with $(\mu_l, \sigma_l) = (0, 4)$. We assumed identical fading and shadowing parameters for both tiers.

Fig. 3 compares the spectral efficiency across a wide range of channel parameters within an interference-limited environment. We observed the following patterns in the spectral efficiency.

1) Strong dominant components or weak scattered components (large κ) achieve a higher rate.
2) Rich scattering with a large number of multipath clusters (large μ) achieves a higher rate.
3) Strong LOS shadowing (small m) achieves a higher rate if $\mu \le 1$ and vice versa.

Large κ and μ parameters indicate strong LOS link and rich multipath components, respectively, both collectively contribute toward increasing the average rate, as illustrated in Figs 3 (a)-(b). On the contrary, the average rate does not show a monotonic behavior for changes in the m parameter. A small value of m implies strong random fluctuation of the dominant component, which decreases not only the received signal power but also the interference level. Based on Figs 3 (c)-(d), it can be observed that the average rate is an increasing function of m if and only if $\mu > 1$ and $\kappa > 16$, where the actual threshold values are determined by the network configuration. Otherwise, the rate is a decreasing function of m. If either the dominant LOS component is weak (small κ) or the number of multipath clusters is small (small μ), LOS shadowing subsides as m increases, which increases the interference power, thus deteriorating the received SINR as well as the average rate.

Figs 4 (a)-(b) compare the spectral efficiency versus the macro BS intensity λ_1. As conjectured in Remark 4, the spectral efficiency becomes invariant for a large BS intensity λ_1. In a dense network with a large BS intensity, the aggregate interference becomes significantly larger than the noise power, achieving an interference-limited condition. Additionally we observe that the BS intensity required to reach the rate asymptote is inversely proportional to the operating SNR level. For a high SNR regime, the average rate reaches the asymptote around $\lambda_1 = 10^{-2}$, whereas in a low SNR regime, a large number of BSs ($\lambda_1 \ge 10^{-1}$) are required to obtain sufficiently larger interference power than the noise. In a sparse network with small BS intensity λ_1, different fading parameters, such as m, do not affect the spectral efficiency significantly. However, in a dense network with a large BS intensity λ_1, different fading parameters have a notable effect on the rate, as illustrated in Figs 4 (a)-(b). This pattern is due to $\Theta(z)$ in (29), which is proportional to $\lambda_0 (1 + \mathcal{W}(z))$ and $\mathcal{W}(z)$ is a function of the channel parameters. If λ_0 (or λ_j) is large, any difference in the channel parameters will be emphasized, affecting the spectral efficiency via $\Theta(z)$. However, if λ_0 is small, any difference in the channel parameters will be unnoticed due to $\lambda_0 (1 + \mathcal{W}(z))$, thus achieving nearly identical network performance. Figs 4 (c)-(d) compare the average SINR across a range of channel parameters assuming an interference-limited environment. We observe that large κ and μ parameters jointly achieve a higher rate similar to Fig. 3.

We also notice that for large κ ($\kappa \ge 15$) and weak shadowing (large m), a higher SINR level is achieved.

VII. CONCLUSION

In this paper, we have considered a cellular network in which the signal fluctuation is the result of large-scale and LOS shadowing to encapsulate the diverse range of channel conditions that can occur in 5G communications. We applied a Laguerre polynomial series expansion to represent the κ-μ shadowed fading distribution as a simplified series expression. Based on the series expressions, we then proposed a novel stochastic geometric method to evaluate the average of an arbitrary function of the SINR over κ-μ shadowed fading channels. The proposed method is numerically efficient, can be easily applied to other network models, and can evaluate any performance measure that can be represented as a function of SINR. Using the proposed method, we have evaluated the spectral efficiency, moments of the SINR, bit error probability and outage probability of a K-tier HetNet with K classes of BSs, differing in terms of the transmit power, BS density, shadowing characteristics and small-scale fading. Furthermore, we provided numerical results and investigated the performance over a range of channel parameters and observed that a dominant LOS component (large κ), rich scattering environment (large μ) and weak shadowing condition (large m) collectively provides high spectral efficiency. Finally, it is worth remarking that the analytical framework proposed in this paper can be applied to practical use cases of 5G communications, where Rayleigh fading fails to fully capture the diverse nature of the underlying channel.

APPENDIX I

In this appendix, we summarize the operational equalities of the special functions, which are used in this paper[7]. First, the generalized Laguerre polynomial of degree n and order β has the following functional identities

$$L_n^\beta(t) = \sum_{i=0}^{n} (-1)^i \binom{n+\beta}{n-i} \frac{t^i}{i!}, \tag{45}$$

$$t^\beta \exp(-t) L_n^\beta(t) dt = \frac{1}{n} d\left[t^{\beta+1} \exp(-t) L_{n-1}^{\beta+1}(t) \right]. \tag{46}$$

The following properties of hypergeometric function hold for real constants a, b and c

$$\begin{aligned} {}_1F_1\left[\begin{matrix} a \\ b \end{matrix} \middle| t \right] &= e^t {}_1F_1\left[\begin{matrix} b-a \\ b \end{matrix} \middle| -t \right], \\ {}_2F_1\left[\begin{matrix} a, b \\ c \end{matrix} \middle| z \right] &= (1-z)^{-a} {}_2F_1\left[\begin{matrix} a, c-b \\ c \end{matrix} \middle| \frac{z}{z-1} \right], \end{aligned} \tag{47}$$

$$\int_0^\infty t^{\alpha-1} e^{-ct} {}_1F_1\left[\begin{matrix} a \\ b \end{matrix} \middle| -t \right] dt = c^{-\alpha} \Gamma(\alpha) {}_2F_1\left[\begin{matrix} a, \alpha \\ b \end{matrix} \middle| -\frac{1}{c} \right] \tag{48}$$
$$\text{for } \alpha > 0 \text{ and } c > 0,$$

[7]Most of the expressions in Appendix I were introduced in [43], except for (53) and (54), which were proved in [37].

$$((a-b)z + c - 2a) \, _2F_1 \begin{bmatrix} a, b \\ c \end{bmatrix} z \end{bmatrix}$$
$$= (c-a) \, _2F_1 \begin{bmatrix} a-1, b \\ c \end{bmatrix} z \end{bmatrix} + a(z-1) \, _2F_1 \begin{bmatrix} a+1, b \\ c \end{bmatrix} z \end{bmatrix}, \quad (49)$$

$$\int_0^\infty e^{-(ax^2+bx)} dx = \frac{1}{2}\sqrt{\frac{\pi}{\alpha}} \exp\left(\frac{b^2}{4a}\right) \mathrm{erfc}\left(\frac{b}{2\sqrt{a}}\right) \quad (50)$$
$$\text{for } a > 0 \text{ and } b > 0.$$

The lower incomplete gamma function $\gamma(s,x) = \int_0^x t^{s-1} e^{-t} dt$ has the following series representation and functional identity for arbitrary positive real constant s

$$\frac{\gamma(s,x)}{\Gamma(s)} = \sum_{n=0}^\infty \frac{x^{s+n} e^{-x}}{\Gamma(s+n+1)}, \quad (51)$$
$$\gamma(s,x) = s^{-1} x^s e^{-x} {}_1F_1 \begin{bmatrix} 1 \\ 1+s \end{bmatrix} x \end{bmatrix}.$$

The binomial coefficient can be defined for real constants x, y using the gamma function as

$$\binom{x}{y} = \frac{\Gamma(x+1)}{\Gamma(y+1)\Gamma(x-y+1)}, \quad \Gamma(t) = \int_0^\infty x^{t-1} e^{-x} dx. \quad (52)$$

Appell's function $F_2(\cdot)$ is defined via the Pochhammer symbol $(x)_n = \frac{\Gamma(x+n)}{\Gamma(x)}$ as follows

$$F_2(\alpha; \beta, \beta'; \gamma, \gamma'; x, y) = \sum_{m=0}^\infty \sum_{n=0}^\infty \frac{(\alpha)_{m+n}(\beta)_m(\beta')_n}{m! \, n! \, (\gamma)_m (\gamma')_n} x^m y^n. \quad (53)$$

Appell's function can be reduced to the hypergeometric function using the following properties

$$F_2(d; a, a'; c, c'; 0, y) = {}_2F_1 \begin{bmatrix} d, a' \\ c' \end{bmatrix} y \end{bmatrix},$$
$$F_2(d; a, a'; c, c'; x, 0) = {}_2F_1 \begin{bmatrix} d, a \\ c \end{bmatrix} x \end{bmatrix}. \quad (54)$$

The following integration holds under the following constraints $d > 0$ and $|k| + |k|' < |h|$

$$\int_0^\infty t^{d-1} e^{-ht} {}_1F_1 \begin{bmatrix} a \\ b \end{bmatrix} kt \end{bmatrix} {}_1F_1 \begin{bmatrix} a' \\ b' \end{bmatrix} k't \end{bmatrix} dt$$
$$= h^{-d} \Gamma(d) F_2\left(d; a, a'; b, b'; \frac{k}{h}, \frac{k'}{h}\right). \quad (55)$$

Gauss-Laguerre quadratures can be used to evaluate the following integral for a given analytic function $g(x)$ as

$$\int_0^\infty e^{-x} g(x) dx = \sum_{n=1}^N w_n f(x_n) + R_N, \quad (56)$$

where x_n and w_n are the n-th abscissa and weight of the N-th order Laguerre polynomial.

APPENDIX II

In this appendix, we provide a proof of Lemma 2. The PDF of h for κ-μ shadowed fading in (10) can be represented in the orthogonal series expansion form as

$$f_h(x) = \sum_{n=0}^\infty C_n \left(\frac{n! \, L_n^{\mu-1}(x)}{\Gamma(n+\mu)}\right) x^{\mu-1} e^{-x}, \quad 0 \le x < \infty, \quad (57)$$

where we applied the Laguerre polynomial series expansion in [34, eq.9] and the coefficient C_n is evaluated by substituting (10) as follows [34, eq.8]

$$C_n = \int_0^\infty L_n^{\mu-1}(x) f_h(x) dx = \frac{\theta_1^{m-\mu}}{\theta_2^m \Gamma(\mu)}$$
$$\times \underbrace{\int_0^\infty x^{\mu-1} e^{-\frac{x}{\theta_1}} L_n^{\mu-1}(x) {}_1F_1 \begin{bmatrix} m \\ \mu \end{bmatrix} \frac{\theta_2 - \theta_1}{\theta_1 \theta_2} x \end{bmatrix} dx}_{I_1}. \quad (58)$$

The integral I_1 can be simplified by using the series representation of $L_n^{\mu-1}(x)$ in (45) as follows

$$I_1 = \sum_{i=0}^n \frac{(-1)^i}{i!} \binom{n+\mu-1}{n-i} \frac{\theta_2^m \Gamma(\mu)}{\theta_1^{m-\mu}} \mathbb{E}\left[h^i\right], \quad (59)$$

where we used (10) to express the integral as the PDF of the κ-μ shadowed fading in the last equality. Then, by substituting (59) into (58), the coefficient C_n in (14) can be derived after algebraic manipulation. The series expansion form in (57) can be further simplified by using (45) and (52) as follows

$$f_h(x) = x^{\mu-1} e^{-x} \sum_{n=0}^\infty \sum_{i=0}^n \frac{n! \, C_n (-1)^i}{\Gamma(n+\mu)} \binom{n+\mu-1}{n-i} \frac{x^i}{i!}$$
$$= \sum_{n=0}^\infty \sum_{i=0}^n \frac{(-1)^i \, C_n}{\Gamma(\mu+i)} \binom{n}{i} x^{\mu+i-1} e^{-x} \quad (60)$$

which achieves (12).

The CDF of h can be evaluated as follows

$$F_h(x) = \int_0^x f_h(t) dt$$
$$= \sum_{n=0}^\infty \frac{n! \, C_n}{\Gamma(n+\mu)} \int_0^x t^{\mu-1} e^{-t} L_n^{\mu-1}(t) dt$$
$$= \sum_{n=1}^\infty \frac{C_n}{(n)_\mu} x^\mu e^{-x} L_{n-1}^\mu(x) + \frac{C_0}{\Gamma(\mu)} \int_0^x t^{\mu-1} e^{-t} L_0^{\mu-1}(t) dt \quad (61)$$
$$= \sum_{n=0}^\infty \sum_{i=0}^n \frac{(-1)^i C_{n+1}}{i! \, (n+1)_\mu} \binom{n+\mu}{n-i} x^{\mu+i} e^{-x} + \frac{\gamma(\mu, x)}{\Gamma(\mu)},$$

where we used (57) in the second equality, utilized (46) in the third equality, applied a change of variable, i.e., $n' \leftarrow n-1$, $C_0 = 1$, $L_0^{\mu-1}(t) = 1$ and (45) in the last equality. The coefficient $b_{i,n}$ can be simplified by using (52) as

$$b_{i,n} = \frac{(-1)^i \Gamma(n+1) C_{n+1}}{i! \, \Gamma(n+\mu+1)} \binom{n+\mu}{n-i} = \frac{(-1)^i C_{n+1}}{\Gamma(\mu+i+1)} \binom{n}{i}, \quad (62)$$

then the CDF in (13) can be subsequently obtained. This completes the proof.

APPENDIX III

In this appendix, we provide a proof of Lemma 3. Due to (2), all interfering BS within the j-th tier are located further than $\hat{P}_j^{\frac{1}{\alpha}} \hat{B}_j^{\frac{1}{\alpha}} \|y_k^*\|$ where y_k^* denote the associated k-th tier BS and $\hat{P}_j = \frac{P_j}{P_k}$ is the transmit power ratio between the interfering and serving BS

$$B_j P_j \|y\|^{-\alpha} < B_k P_k \|y_k^*\|^{-\alpha} \text{ for any } y \in \Phi_j^{(e)} \backslash \{y_k^*\}$$
$$\Leftrightarrow \|y\| > \hat{B}_j^{\frac{1}{\alpha}} \hat{P}_j^{\frac{1}{\alpha}} \|y_k^*\|. \quad (63)$$

$$\mathcal{L}_{I_j}(s) = \mathbb{E}\left[\exp\left(-s\sum_{y\in\Phi_j^{(e)}\setminus\{y_k^*\}}\hat{P}_j h_y\|y\|^{-\alpha}\right)\right] = \exp\left[-2\pi\lambda_j\mathbb{E}[\chi_j^\delta]\int_{\hat{B}_j^{\frac{1}{\alpha}}\hat{P}_j^{\frac{1}{\alpha}}r}^\infty\left(1-\mathbb{E}_h\left[\exp\left(-s\hat{P}_j hl^{-\alpha}\right)\right]\right)l\,\mathrm{d}l\right]$$

$$= \exp\left[-\pi\lambda_j\mathbb{E}[\chi_j^\delta]\hat{B}_j^\delta\hat{P}_j^\delta\ \mathbb{E}_h\left\{(sh)^\delta\int_0^{shr^{-\alpha}}\delta t^{-\delta-1}(1-\mathrm{e}^{-t})\mathrm{d}t\right\}\right]$$

$$= \exp\left[-\pi r^2\lambda_j\mathbb{E}[\chi_j^\delta]\hat{B}_j^\delta\hat{P}_j^\delta\ \mathbb{E}_h\left\{(shr^{-\alpha})^\delta\gamma(1-\delta,shr^{-\alpha})-\left(1-\mathrm{e}^{-shr^{-\alpha}}\right)\right\}\right],\qquad(64)$$

$$\mathbb{E}_h\left[(shr^{-\alpha})^\delta\gamma(1-\delta,shr^{-\alpha})\right] = \frac{(s\theta_1 r^{-\alpha})^\delta}{\Gamma(\mu)}\left(\frac{\theta_1}{\theta_2}\right)^m\int_0^\infty t^{\delta+\mu-1}\mathrm{e}^{-t}{}_1F_1\left[\begin{matrix}m\\\mu\end{matrix}\,\bigg|\,\frac{\mu\kappa}{\mu\kappa+m}t\right]\gamma(1-\delta,s\theta_1 r^{-\alpha}t)\mathrm{d}t$$

$$= \frac{s\theta_1 r^{-\alpha}(\theta_1/\theta_2)^m}{(1-\delta)\Gamma(\mu)}\int_0^\infty t^\mu\mathrm{e}^{-(1+s\theta_1 r^{-\alpha})t}{}_1F_1\left[\begin{matrix}m\\\mu\end{matrix}\,\bigg|\,\frac{\mu\kappa}{\mu\kappa+m}t\right]{}_1F_1\left[\begin{matrix}1\\2-\delta\end{matrix}\,\bigg|\,s\theta_1 r^{-\alpha}t\right]\mathrm{d}t\qquad(65)$$

$$= \frac{\mu}{(1-\delta)}\frac{s\theta_1 r^{-\alpha}}{(1+s\theta_1 r^{-\alpha})^{\mu+1}}\left(\frac{\theta_1}{\theta_2}\right)^m F_2(\mu+1;m,1;\mu,2-\delta;A,B),$$

$$\mathcal{W}_j(z) = \frac{(s\theta_1 r^{-\alpha})^\delta}{\Gamma(\mu)}\left(\frac{\theta_1}{\theta_2}\right)^m\int_0^\infty t^{\delta+\mu-1}\mathrm{e}^{-t}{}_1F_1\left[\begin{matrix}m\\\mu\end{matrix}\,\bigg|\,\frac{\mu\kappa}{\mu\kappa+m}t\right]\gamma(1-\delta,s\theta_1 r^{-\alpha}t)\mathrm{d}t - (1-(1+\theta_1 z)^{m-\mu}(1+\theta_2 z)^{-m})$$

$$\approx \frac{(\theta_1 z)^\delta}{\Gamma(\mu)}\left(\frac{\theta_1}{\theta_2}\right)^m\sum_{n=1}^N w_n f(x_n) - (1-(1+\theta_1 z)^{m-\mu}(1+\theta_2 z)^{-m}).\qquad(66)$$

The Laplace transform of the interference from the j-th tier is derived in (64), where we represented the distance to the serving BS as $\|y_k^*\| = r$ in the second equality, applied a change of variable, i.e., $s\hat{P}_j\hat{B}_j hl^{-\alpha} = t$, in the third equality, then used integration by parts. The first part of the expectation term in (64) is evaluated by (65), where we used the PDF of κ-μ shadowed fading with a change of variable, i.e., $\frac{h}{\theta_1} = t$ in the first equality, applied (51) to the second equality, utilized the integration (55) in the last equality [37], $A = \frac{1-\theta_1/\theta_2}{1+\theta_1 sr^{-\alpha}}$ and $B = \frac{\theta_1 sr^{-\alpha}}{1+\theta_1 sr^{-\alpha}}$. The second part of the expectation term in (64) follows directly by using the Laplace transform of κ-μ shadowed channel coefficient (10). By denoting $sr^{-\alpha} = z$, (16) and (17) can be achieved. This completes the proof.

APPENDIX IV

All numerical results provided in this paper are obtained by using Julia language [42] and we used `appellf2` function in SymPy package [44] to evaluate the Appell's function in (17). However, if one needs to use MATLAB, where a native Appell's function library do not exist yet, $\mathcal{W}_j(z)$ can be accurately approximated by using the Gauss-Laguerre Quadrature as (66), where $f(x) = x^{\delta+\mu-1}{}_1F_1\left[\begin{matrix}m\\\mu\end{matrix}\,\big|\,\frac{\mu\kappa}{\mu\kappa+m}x\right]\gamma(1-\delta,\theta_1 zx)$, x_n and w_n are the n-th abscissa and weight of the N-th order Laguerre polynomial. Since the approximation error converges rapidly to zero [43], (66) provides a numerically accurate and efficient approximation to $\mathcal{W}_j(z)$.

APPENDIX V

In this appendix, we provide a proof of Lemma 5. First, we consider Nakagami-m fading which corresponds to the case when $\kappa \to 0, \mu = m$ in Table 1. Then $\theta_1 = \theta_2 = \frac{\bar{h}}{m}$ and

$A = \frac{1-\theta_1/\theta_2}{1+\theta_1 z} \to 0$. By applying (54) and (47), (17) can be simplified to the following form

$$F_2(\mu+1;m,1;\mu,2-\delta;A,B)$$
$$= (1+\theta_1 z)^{\mu+1}{}_2F_1\left[\begin{matrix}\mu+1,1-\delta\\2-\delta\end{matrix}\,\bigg|\,-\theta_1 z\right].\qquad(67)$$

$\mathcal{W}_j(z)$ for Nakagami-m fading can be obtained by substituting (67) in (17) with $\kappa \to 0, \mu = m$. For One-sided Gaussian fading, (21) is obtained by substituting $\mu = 0.5$ in (20). $\mathcal{W}_j(z)$ for Rayleigh fading in (19) can be obtained by substituting $\mu = 1$ in (20), then applying (49) and ${}_2F_1\left[\begin{matrix}0,b\\c\end{matrix}\,\big|\,x\right] = 1$, which achieves an identical result to [7, eq. (44)].

Next, we show that κ-μ fading corresponds to the case of $m \to \infty$ with the following limit

$$\lim_{m\to\infty}\left(\frac{\theta_1}{\theta_2}\right)^m = \lim_{m\to\infty}\left(1+\frac{\mu\kappa}{m}\right)^{-m} = \mathrm{e}^{-\mu\kappa}$$

$$\lim_{m\to\infty}\left(\frac{1+\theta_1 s}{1+\theta_2 s}\right)^m = \lim_{m\to\infty}\left(1+\frac{\mu\kappa s}{m(s+\theta_1^{-1})}\right)^{-m}\qquad(68)$$

$$= \exp\left(-\frac{\mu\kappa s}{s+\theta_1^{-1}}\right).$$

By utilizing (68) and (67) in (17), (22) can be derived for $m \to \infty$. $\mathcal{W}_j(z)$ for Rician fading readily follows by substituting $\kappa = K$ and $\mu = 1$ in (22). This completes the proof.

APPENDIX VI

In this appendix, we provide a proof of Theorem 1. The average of an arbitrary function of the SINR $\frac{h_{x_0}\|x_0\|^{-\alpha}}{I+N}$ is evaluated in (69), where (12) is used in the second equality, a change of variable, i.e., $\frac{xr^{-\alpha}}{I+N} = z$, is utilized in the third

$$\mathbb{E}\left[g\left(\frac{h_{x_0}r^{-\alpha}}{I+N}\right)\Big| I, \|x_0\|=r\right] = \int_0^\infty g\left(\frac{xr^{-\alpha}}{I+N}\right)f_h(x)\mathrm{d}x = \sum_{n=0}^\infty \sum_{i=0}^n c_{i,n}\int_0^\infty x^{\mu+i-1}\mathrm{e}^{-x}g\left(\frac{xr^{-\alpha}}{I+N}\right)\mathrm{d}x$$

$$= \sum_{n=0}^\infty \sum_{i=0}^n c_{i,n}\int_0^\infty z^{\mu+i-1}g(z)(r^\alpha(I+N))^{\mu+i}\mathrm{e}^{-r^\alpha(I+N)z}\mathrm{d}z \tag{69}$$

$$= \sum_{n=0}^\infty C_n \sum_{i=0}^n (-1)^i\binom{n}{i}\int_0^\infty \frac{z^{\mu+i-1}g(z)}{\Gamma(\mu+i)}(r^\alpha(I+N))^{\mu+i}\mathrm{e}^{-r^\alpha(I+N)z}\mathrm{d}z,$$

$$\mathbb{E}\left[g\left(\frac{h_{x_0}\|x_0\|^{-\alpha}}{I+N}\right)\right] = \mathbb{E}\left[\mathbb{E}\left[g\left(\frac{h_{x_0}r^{-\alpha}}{I+N}\right)\Big|\|x_0\|=r\right]\right]$$

$$= \sum_{n=0}^\infty C_n \sum_{i=0}^n (-1)^i\binom{n}{i}\int_0^\infty g_{\mu+i}(z)\mathrm{e}^{-r^\alpha Nz}\mathcal{L}_I(r^\alpha z)f_{\|x_0\|}(r)\mathrm{d}r, \tag{70}$$

$$\mathbb{E}_r\left[\mathrm{e}^{-r^\alpha\hat{N}z}\mathcal{L}_I(r^\alpha z)\right] = \int_0^\infty \mathrm{e}^{-r^\alpha\hat{N}z}\mathcal{L}_I(r^\alpha z)f_{\|y_k^*\|}(r)\mathrm{d}r$$

$$= \frac{2\pi\lambda_k\mathbb{E}\left[\chi_k^\delta\right]}{\mathcal{P}_k}\int_0^\infty r\,\mathrm{e}^{-r^\alpha\hat{N}z}\exp\left[-\sum_{j\in\mathcal{K}}\pi r^2\lambda_j\mathbb{E}\left[\chi_j^\delta\right]\hat{P}_j^\delta\hat{B}_j^\delta\left(1+\mathcal{W}_j(z)\right)\right]\mathrm{d}r \tag{71}$$

$$= \frac{\lambda_k\mathbb{E}\left[\chi_k^\delta\right]}{\mathcal{P}_k}\int_0^\infty \exp\left[-t^{\frac{1}{\delta}}\frac{\hat{N}z}{\pi^{\frac{\alpha}{2}}}-t\left(\sum_{j\in\mathcal{K}}\lambda_j\mathbb{E}\left[\chi_j^\delta\right]\hat{P}_j^\delta\hat{B}_j^\delta\left(1+\mathcal{W}_j(z)\right)\right)\right]\mathrm{d}r.$$

equality, and (14) is employed in the last equality. (69) can be evaluated as follows

$$\int_0^\infty \underbrace{\frac{z^{\mu+i-1}}{\Gamma(\mu+i)}g(z)}_{u}\underbrace{b^{\mu+i}\mathrm{e}^{-bz}}_{v'}\mathrm{d}x$$

$$= -\sum_{k=0}^{\mu+i-1}g_k(z)b^{\mu+i-k-1}\mathrm{e}^{-bz}\Big|_0^\infty + \int_0^\infty g_{\mu+i}(z)\mathrm{e}^{-bz}\mathrm{d}z, \tag{72}$$

where we denoted $b = r^\alpha(I+N)$, applied integration by parts, defined $g_k(z)$ in (26), and

$$g_k(0) = \begin{cases}0, & \text{for } k < \mu+i-1 \\ g(0), & \text{for } k = \mu+i-1\end{cases}. \tag{73}$$

Then, the average of an arbitrary function of the SINR is given by (70), where we used $\sum_{i=0}^n(-1)^i\binom{n}{i}=0$ in the second equality. This completes the proof.

APPENDIX VII

In this appendix, we provide proof of Lemmas 6, 7 and 8. By substituting (4) and (16) to (25), the expectation term $\mathbb{E}_r\left[\mathrm{e}^{-r^\alpha\hat{N}z}\mathcal{L}_I(r^\alpha z)\right]$ can be evaluated as (71), where we used a change of variable, i.e., $t = \pi r^2$ in the last equality. If $\alpha = 4$, then (28) can be achieved by applying (50). Given an interference-limited condition, (71) reduces to

$$\frac{\lambda_k\mathbb{E}\left[\chi_k^\delta\right]}{\mathcal{P}_k}\int_0^\infty \mathrm{e}^{-t\left(\sum_{j\in\mathcal{K}}\lambda_j\mathbb{E}\left[\chi_j^\delta\right]\hat{P}_j^\delta\hat{B}_j^\delta(1+\mathcal{W}_j(z))\right)}\mathrm{d}r$$

$$= \frac{\lambda_k\mathbb{E}\left[\chi_k^\delta\right]/\mathcal{P}_k}{\sum_{j\in\mathcal{K}}\lambda_j\mathbb{E}\left[\chi_j^\delta\right]\hat{P}_j^\delta\hat{B}_j^\delta\left(1+\mathcal{W}_j(z)\right)}, \tag{74}$$

whereas for noise-limited condition, (71) can be written as

$$\frac{\lambda_k\mathbb{E}\left[\chi_k^\delta\right]}{\mathcal{P}_k}\int_0^\infty \exp\left[-t^{\frac{1}{\delta}}\frac{\hat{N}z}{\pi^{\frac{\alpha}{2}}}-t\sum_{j\in\mathcal{K}}\lambda_j\mathbb{E}\left[\chi_j^\delta\right]\hat{P}_j^\delta\hat{B}_j^\delta\right]\mathrm{d}r. \tag{75}$$

(32) readily follows by substituting $\mathcal{W}_j(z)\to 0$ and $\alpha = 4$ in (28). This completes the proof.

## REFERENCES

[1] 5GPPP, "5G empowering vertical industries," Tech. Rep., 2016.
[2] Nokia White Paper, "5G use cases and requirements," Tech. Rep., 2014.
[3] M. Haenggi, *Stochastic geometry for wireless networks*. Cambridge University Press, 2012.
[4] J. G. Andrews, R. K. Ganti, M. Haenggi, N. Jindal, and S. Weber, "A primer on spatial modeling and analysis in wireless networks," *IEEE Commun. Mag.*, vol. 48, no. 11, pp. 156–163, 2010.
[5] R. Mathar and J. Mattfeldt, "On the distribution of cumulated interference power in Rayleigh fading channels," *Wirel. Networks*, vol. 1, no. 1, pp. 31–36, 1995.
[6] J. G. Andrews, F. Baccelli, and R. K. Ganti, "A tractable approach to coverage and rate in cellular networks," *IEEE Trans. Commun.*, vol. 59, no. 11, pp. 3122–3134, 2011.
[7] H. S. Jo, Y. J. Sang, P. Xia, and J. G. Andrews, "Heterogeneous cellular networks with flexible cell association: a comprehensive downlink SINR analysis," *IEEE Trans. Wirel. Commun.*, vol. 11, no. 10, pp. 3484–3494, 2012.
[8] S. Mukherjee, "Distribution of downlink SINR in heterogeneous cellular networks," *IEEE J. Sel. Areas Commun.*, vol. 30, no. 3, pp. 575–585, 2012.
[9] H. S. Dhillon, R. K. Ganti, F. Baccelli, and J. G. Andrews, "Modeling and analysis of K-tier downlink heterogeneous cellular networks," *IEEE J. Sel. Areas Commun.*, vol. 30, no. 3, pp. 550–560, 2012.
[10] Y. Chun, M. Hasna, and A. Ghrayeb, "Modeling heterogeneous cellular networks interference using poisson cluster processes," *IEEE J. Sel. Areas Commun.*, vol. 33, no. 10, pp. 1–1, 2015.
[11] C. Saha, M. Afshang, and H. S. Dhillon, "Enriched K-tier HetNet model to enable the analysis of user-centric small cell deployments," *IEEE Trans. Wirel. Commun.*, vol. 16, no. 3, pp. 1593–1608, 2017.

This article has been accepted for publication in a future issue of this journal, but has not been fully edited. Content may change prior to final publication. Citation information: DOI 10.1109/TWC.2017.2734080, IEEE Transactions on Wireless Communications

15

[12] J. G. Andrews, A. K. Gupta, and H. S. Dhillon, "A primer on cellular network analysis using stochastic geometry," pp. 1–38, 2016. [Online]. Available: http://arxiv.org/abs/1604.03183

[13] H. Elsawy, E. Hossain, and M. Haenggi, "Stochastic geometry for modeling, analysis, and design of multi-tier and cognitive cellular wireless networks: A survey," *IEEE Commun. Surv. Tutorials*, vol. 15, no. 3, pp. 996–1019, 2013.

[14] M. Haenggi, J. G. Andrews, F. Baccelli, O. Dousse, and M. Franceschetti, "Stochastic geometry and random graphs for the analysis and design of wireless networks," *IEEE J. Sel. Areas on Commun.*, no. 7, pp. 1029–1046.

[15] B. Blaszczyszyn and H. P. Keeler, "Equivalence and comparison of heterogeneous cellular networks," *IEEE Int. Symp. Pers. Indoor Mob. Radio Commun. PIMRC*, pp. 153–157, 2013.

[16] H. P. Keeler, B. Blaszczyszyn, and M. K. Karray, "SINR-based k-coverage probability in cellular networks with arbitrary shadowing," *IEEE Int. Symp. Inf. Theory - Proc.*, pp. 1167–1171, 2013.

[17] P. Madhusudhanan, J. G. Restrepo, Y. Liu, T. X. Brown, and K. R. Baker, "Downlink performance analysis for a generalized shotgun cellular system," *IEEE Trans. Wirel. Commun.*, vol. 13, no. 12, pp. 6684–6696, 2014.

[18] H. S. Dhillon and J. G. Andrews, "Downlink rate distribution in heterogeneous cellular networks under generalized cell selection," *IEEE Wirel. Commun. Lett.*, vol. 3, no. 1, pp. 42–45, 2014.

[19] X. Zhang and M. Haenggi, "A stochastic geometry analysis of inter-cell interference coordination and intra-cell diversity," *IEEE Trans. Wirel. Commun.*, vol. 13, no. 12, pp. 6655–6669, 2014.

[20] M. Peng, Y. Li, T. Q. S. Quek, and C. Wang, "Device-to-device underlaid cellular networks under rician fading channels," *IEEE Trans. Wirel. Commun.*, vol. 13, no. 8, pp. 4247–4259, 2014.

[21] R. Tanbourgi, H. S. Dhillon, J. G. Andrews, and F. K. Jondral, "Dual-branch MRC receivers under spatial interference correlation and Nakagami fading," *IEEE Trans. Commun.*, vol. 62, no. 6, pp. 1830–1844, 2014.

[22] G. Miel and R. Mooney, "On the condition number of Lagrangian numerical differentiation," *Appl. Math. Comput.*, vol. 16, no. 3, pp. 241–252, 1985.

[23] M.-J. Ho and G. Stuber, "Co-channel interference of microcellular systems on shadowed Nakagami fading channels," *IEEE 43rd Veh. Technol. Conf.*, pp. 568–571, 1993.

[24] A. Abdi and M. Kaveh, "K distribution: an appropriate substitute for Rayleigh-lognormal distribution in fading-shadowing wireless channels," *Electron. Lett.*, vol. 34, no. 9, pp. 851–852, 1998.

[25] A. Abdi, W. C. Lau, M. S. Alouini, and M. Kaveh, "A new simple model for land mobile satellite channels: first- and second-order statistics," *Wirel. Commun. IEEE Trans.*, vol. 2, no. 3, pp. 519–528, 2003.

[26] J. F. Paris, "Statistical characterization of κ-μ Shadowed fading," *IEEE Trans. Veh. Technol.*, vol. 63, no. 2, pp. 518–526, 2014.

[27] S. L. Cotton, "Human body shadowing in cellular device-to-device communications: channel modeling using the shadowed $\kappa - \mu$ fading model," *IEEE J. Sel. Areas Commun.*, vol. 33, no. 1, pp. 111–119, 2015.

[28] A. Sánchez, E. Robles, F. Rodrigo, F. Ruiz-Vega, U. Fernández-Plazaola, and J. Paris, "Measurement and modeling of fading in ultrasonic underwater Channels," *Int. Conf. Exhib. Underw. Acoust.*, pp. 1213–1218, 2014.

[29] S. L. Cotton, "Shadowed fading in body-to-body communications channels in an outdoor environment at 2.45 GHz," in *2014 IEEE-APS Top. Conf. Antennas Propag. Wirel. Commun.*, vol. 44, no. 0. IEEE, 2014, pp. 249–252.

[30] M. K. Simon and M.-S. Alouini, *Digital Communication over Fading Channels*. Wiley-IEEE Press, 2004.

[31] L. Moreno-Pozas, F. J. Lopez-Martinez, J. F. Paris, and E. Martos-Naya, "The κ-μ shadowed fading model: unifying the κ-μ and η-μ distributions," *IEEE Trans. Veh. Technol.*, vol. 65, no. 12, pp. 9630–9641, 2016.

[32] S. Kumar, "Approximate outage probability and capacity for κ-μ shadowed fading," *IEEE Wirel. Commun. Lett.*, vol. 4, no. 3, pp. 301–304, 2015.

[33] S. Parthasarathy and R. K. Ganti, "Coverage analysis in downlink poisson cellular network with κ-μ shadowed fading," *IEEE Wirel. Commun. Lett.*, vol. 6, no. 1, pp. 10–13, 2016.

[34] C. Chai and T. Tjhung, "Unified Laguerre polynomial-series-based distribution of small-scale fading envelopes," *IEEE Trans. Veh. Technol.*, vol. 58, no. 8, pp. 3988–3999, 2009.

[35] A. Abdi, "On the utility of Laguerre series for the envelope pdf in multipath fading channels," *IEEE Trans. Inf. Theory*, vol. 55, no. 12, pp. 5652–5662, 2009.

[36] F. J. Lopez-Martinez, J. F. Paris, and J. M. Romero-Jerez, "The κ-μ shadowed fading model with integer fading parameters," *IEEE Trans. Veh. Technol., to appear*, 2017.

[37] N. Saad and R. L. Hall, "Integrals containing confluent hypergeometric functions with applications to perturbed singular potentials," *J. Phys. A Math.*, vol. 36, no. June, p. 20, 2003.

[38] K. A. Hamdi, "A useful technique for interference analysis in Nakagami fading," *IEEE Trans. Commun.*, vol. 55, no. 6, pp. 1120–1124, 2007.

[39] Y. J. Chun, S. L. Cotton, H. S. Dhillon, A. Ghrayeb, and M. O. Hasna, "A stochastic geometric analysis of device-to-device communications operating over generalized fading channels," *IEEE Trans. Wirel. Commun.*, vol. 16, no. 7, pp. 4151–4165, July 2017.

[40] A. A. Minai and R. D. Williams, "On the derivatives of the sigmoid," *Neural Networks*, vol. 6, no. 6, pp. 845–853, 1993.

[41] M. Di Renzo and P. Guan, "Stochastic geometry modeling of coverage and rate of cellular networks using the Gil-Pelaez inversion theorem," *IEEE Commun. Lett.*, vol. 18, no. 9, pp. 1575–1578, 2014.

[42] J. Bezanson, A. Edelman, S. Karpinski, and V. B. Shah, "Julia: a fresh approach to numerical computing," *SIAM Rev.*, vol. 59, no. 1, pp. 65–98, 2017.

[43] I. S. Gradshteyn and I. M. Ryzhik, *Table of integrals, series, and products*, 5th ed. Academic Press, 1994.

[44] "SymPy." [Online]. Available: http://www.sympy.org/en/index.html

Young Jin Chun received the B.S. degree from Yonsei University, Seoul, South Korea, in 2004, the M.S. degree from the University of Michigan, Ann Arbor, in 2007, and the Ph.D. degree from Iowa State University, Ames, in 2011, all in electrical engineering. He was a Post-Doctoral Researcher with Sungkyunkwan University, Suwon, South Korea, from 2011 to 2012, and with Qatar University, Doha, Qatar, from 2013 to 2014. In 2015, he joined Queen's University Belfast, U.K. as a Research Fellow. His research interests are primarily in the area of wireless communications with emphasis on stochastic geometry, system-level network analysis, device-to-device communications, and various use cases of 5G communications.
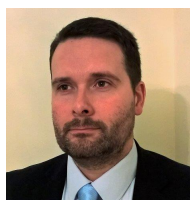
Simon L. Cotton (S'04–M'07–SM'14) received the B.Eng. degree in electronics and software from Ulster University, Ulster, U.K., in 2004, and the Ph.D. degree in electrical and electronic engineering from the Queen's University of Belfast, Belfast, U.K., in 2007. He is currently a Reader of Wireless Communications with the Institute of Electronics, Communications and Information Technology, Queen's University Belfast, and also a Co-Founder and the Chief Technology Officer with ActivWireless Ltd., Belfast. He has authored and co-authored over 100 publications in major IEEE/IET journals and refereed international conferences, two book chapters, and two patents. Among his research interests are cellular device-to-device, vehicular, and body-centric communications. His other research interests include radio channel characterization and modeling and the simulation of wireless channels. He was a recipient of the H. A. Wheeler Prize, in 2010, from the IEEE Antennas and Propagation Society for the best applications journal paper in the IEEE TRANSACTIONS ON ANTENNAS AND PROPAGATION in 2009. In 2011, he was a recipient of the Sir George Macfarlane Award from the U.K. Royal Academy of Engineering in recognition of his technical and scientific attainment since graduating from his first degree in engineering.

This article has been accepted for publication in a future issue of this journal, but has not been fully edited. Content may change prior to final publication. Citation information: DOI 10.1109/TWC.2017.2734080, IEEE Transactions on Wireless Communications

16

Harpreet S. Dhillon (S'11–M'13) received the B.Tech. degree in Electronics and Communication Engineering from IIT Guwahati, India, in 2008; the M.S. degree in Electrical Engineering from Virginia Tech, Blacksburg, VA, USA, in 2010; and the Ph.D. degree in Electrical Engineering from the University of Texas at Austin, TX, USA, in 2013. After a postdoctoral year at the University of Southern California (USC), Los Angeles, CA, USA, he joined Virginia Tech in August 2014, where he is currently an Assistant Professor of Electrical and Computer Engineering. He has held internships at Alcatel-Lucent Bell Labs in Crawford Hill, NJ, USA; Samsung Research America in Richardson, TX, USA; Qualcomm Inc. in San Diego, CA, USA; and Cercom, Politecnico di Torino in Italy. His research interests include communication theory, stochastic geometry, geolocation, and wireless *ad hoc* and heterogeneous cellular networks.

Dr. Dhillon has been a co-author of five best paper award recipients including the 2016 IEEE Communications Society (ComSoc) Heinrich Hertz Award, the 2015 IEEE ComSoc Young Author Best Paper Award, the 2014 IEEE ComSoc Leonard G. Abraham Prize, the 2014 European Wireless Best Student Paper Award, and the 2013 IEEE International Conference in Communications Best Paper Award in the Wireless Communications Symposium. He was also the recipient of the USC Viterbi Postdoctoral Fellowship, the 2013 UT Austin Wireless Networking and Communications Group (WNCG) leadership award, the UT Austin Microelectronics and Computer Development (MCD) Fellowship, and the 2008 Agilent Engineering and Technology Award. He currently serves as an Editor for the IEEE TRANSACTIONS ON WIRELESS COMMUNICATIONS, the IEEE TRANSACTIONS ON GREEN COMMUNICATIONS AND NETWORKING, and the IEEE WIRELESS COMMUNICATIONS LETTERS. In 2017, he was named the Outstanding New Assistant Professor by the Virginia Tech College of Engineering.

Jose F. Paris (M'12–SM'16) received the M.Sc. and Ph.D. degrees in telecommunication engineering from the Universidad de Malaga, Spain, in 1996 and 2004, respectively. From 1994 to 1996 he was with Alcatel, mainly in the development of wireless telephones. In 1997, he joined the Universidad de Malaga, where is currently an Associate Professor with the Communication Engineering Department. His teaching activities include several courses on digital communications, signal processing, and acoustic engineering. His research interests are related to wireless communications, especially channel modeling, and performance analysis.

In 2005, he spent five months as a Visiting Associate Professor with Stanford University, with Prof. A. J. Goldsmith. In 2014, he obtained the Full Professor (Catedratico de Universidad) certification by the Spanish Ministry of Education. He received the 2016 Neil Shepherd Memorial Best Propagation Paper Award by the IEEE Vehicular Technology Society. He serves as an Associate Editor of the IEEE COMMUNICATIONS LETTERS, and the IEEE TRANSACTIONS ON VEHICULAR TECHNOLOGY.

Seong Ki Yoo received the B.Eng. (Hons.) degree in telecommunication systems from the University of Surrey, Guildford, U.K., in 2010, and the M.Sc. degree in communications and signal processing from Imperial College London, London, U.K., in 2012. He is currently pursuing the Ph.D. degree with Queen's University Belfast, Belfast, U.K. His Ph.D. studies have been sponsored by U.K. EPSRC. His research interests are in the areas of fading channel characterization and modeling for wearable communications and diversity in wearable applications.

F. Javier Lopez-Martinez (S'05–M'10) received the M.Sc. and Ph.D. degrees in telecommunication engineering from the University of Malaga, Spain, in 2005 and 2010, respectively. He joined the Communication Engineering Department, University of Malaga, as an Associate Researcher, in 2005. In 2010, he was a Visitor Researcher with University College London. He was a Marie Curie PostDoctoral Fellow with the Wireless Systems Laboratory, Stanford University, from 2012 to 2014. He joined the Universidad de Malaga in 2014 and has been an Assistant Professor with the Communication Engineering Department since 2015. His research interests span a diverse set of topics in the wide areas of communication theory and wireless communications: stochastic processes, wireless channel modeling, random matrix theory, physical layer security, massive MIMO, and mm-wave for 5G. He has received several research awards, including the Best Paper Award in the Communication Theory Symposium at the IEEE GLOBECOM 2013, the IEEE COMMUNICATIONS LETTERS Exemplary Reviewer Certificate in 2014, and the IEEE TRANSACTIONS ON COMMUNICATIONS Exemplary Reviewer Certificate in 2015 and 2017. He is an Editor of the IEEE TRANSACTIONS ON COMMUNICATIONS in the area of Wireless Communications.